AD-762 282

HIGH LATITUDE MODELS, OBSERVATIONS, AND ANALYSIS OF IONOSPHERIC SCINTILLATIONS

Jules Aarons, et al

Air Force Cambridge Research Laboratories
L. G. Hanscom Field, Massachusetts

12 January 1973

AD 762282

AIR FORCE CAMBRIDGE RESEARCH LABORATORIES

L. G. HANSCOM FIELD, BEDFORD, MASSACHUSETTS

High Latitude Models, Observations, and Analysis of Ionospheric Scintillations

JULES AARONS
HERBERT E. WHITNEY
RICHARD S. ALLEN
DOUGLAS R. SEEMANN

AIR FORCE SYSTEMS COMMAND

United States Air Force

NATIONAL TECHNICAL
INFORMATION SERVICE

Best Available Copy

65

AIR FORCE CAMBRIDGE RESEARCH LABORATORIES

L. G. HANSCOM FIELD, BEDFORD, MASSACHUSETTS

High Latitude Models, Observations, and Analysis of Ionospheric Scintillations

JULES AARONS
HERBERT E. WHITNEY
RICHARD S. ALLEN
DOUGLAS R. SEEMANN

AIR FORCE SYSTEMS COMMAND
United States Air Force

DOCUMENT CONTROL DATA - R&D

(Security classification of title, body of abstract and indexing annotation must be entered when the overall report is classified)

1. ORIGINATING ACTIVITY *(Corporate author)*	2a. REPORT SECURITY CLASSIFICATION
Air Force Cambridge Research Laboratories (LI) L. G. Hanscom Field Bedford, Massachusetts 01730	Unclassified
	2b. GROUP

3. REPORT TITLE

HIGH LATITUDE MODELS, OBSERVATIONS, AND ANALYSIS OF IONOSPHERIC SCINTILLATIONS

4. DESCRIPTIVE NOTES *(Type of report and inclusive dates)*

Scientific. Interim.

5. AUTHOR(S) *(First name, middle initial, last name)*

Jules Aarons   Richard S. Allen
Herbert E. Whitney   Douglas R. Seemann

6. REPORT DATE	7a. TOTAL NO. OF PAGES	7b. NO. OF REFS
12 January 1973	64	33

8a. CONTRACT OR GRANT NO.	9a. ORIGINATOR'S REPORT NUMBER(S)
b. PROJECT, TASK, WORK UNIT NOS. 4643-01-01	AFCRL-TR-73-0048
c. DOD ELEMENT 62101F	9b. OTHER REPORT NO(S) *(Any other numbers that may be assigned this report)*
d. DOD SUBELEMENT 681000	AFSG No. 254

10. DISTRIBUTION STATEMENT

Approved for public release; distribution unlimited.

11. SUPPLEMENTARY NOTES	12. SPONSORING MILITARY ACTIVITY
TECH, OTHER	Air Force Cambridge Research Laboratories (LI) L. G. Hanscom Field Bedford, Massachusetts 01730

13. ABSTRACT

In order to provide systems engineers with observations and analysis of the amplitude-fading of radio waves traversing the high latitude ionosphere, several different studies were performed. The concept was to develop descriptive and statistical models for the pattern of occurrence and amplitude of scintillations at high latitudes. Then, long term observations from a limited number of sites could be linked to allow an assessment of the scintillation problem to communication, navigation, and detection systems in the VHF and UHF bands. This report discusses these studies in three chapters. In Chapter 1, general patterns of scintillation occurrence and intensity are presented in the descriptive model of the F-layer irregularities at high latitudes. This is followed in Chapter 2 by a graphical presentation of the data; that is, observations of the 136 MHz beacon of ATS-3. Chapter 3 organizes the observations into a useful format—the cumulative amplitude probability distribution function—for the engineer. A means of adjusting the observations for frequency dependence is provided. Cumulative amplitude probabilities are listed for Sagamore Hill, Massachusetts and Narssarssuaq, Greenland as a function of season, time and K index. For Thule, Greenland cumulative amplitude probability distributions are listed for ATS-3 at 136 MHz. With this data and with the descriptive model, it is proposed that the engineer can evaluate the effect of scintillations on systems operating in auroral and polar regions.

DD FORM 1473, 1 NOV 65

14. KEY WORDS	LINK A		LINK B		LINK C	
	ROLE	WT	ROLE	WT	ROLE	WT
Amplitude fading						
F-layer irregularities						
Scintillations						

Abstract

In order to provide systems engineers with observations and analysis of the anplitude-fading of radio waves traversing the high latitude ionosphere, several different studies were performed. The concept was to .... descriptive and statistical models for the pattern of occurrence and amplitude of scintillations at high latitudes. Then, long term observations from a limited number of sites could be linked to allow an assessment of the scintillation problem to communication, navigation, and detection systems in the VHF and UHF bands. This report discusses these studies in three chapters. In Chapter 1, general patterns of scintillation occurrence and intensity are presented in the descriptive model of the F-layer irregularities at high latitudes. This is followed in Chapter 2 by a graphical presentation of the data; that is, observations of the 136 MHz beacon of ATS-3. Chapter 3 organizes the observations into a useful format—the cumulative amplitude probability distribution function—for the engineer. A means of adjusting the observations for frequency dependence is provided. Cumulative amplitude probabilities are listed for Sagamore Hill, Massachusetts and Narssarssuaq, Greenland as a function of season, time and K index. For Thule, Greenland cumulative amplitude probability distributions are listed for ATS-3 at 136 MHz. With this data and with the descriptive model, it is pr posed that the engineer can evaluate the effect of scintillations on systems operating in auroral and polar regions.

Contents

v

Contents

HIGH LATITUDE MODELS, OBSERVATIONS, AND ANALYSIS OF IONOSPHERIC SCINTILLATIONS

1. A Descriptive Model of F-Layer High Latitude Irregularities

Jules Aarons
Radio Astronomy Branch
Ionospheric Physics Laboratory
Air Force Cambridge Research Laboratories
Bedford, Massachusetts

Abstract

Using observations of the amplitude fluctuations of radio signals from satellites and radio stars as a data base, a model is sketched of the high latitude F-layer irregularity region. The irregularities of concern are field aligned and small scale (1 to 10 km). On the nightside, irregularity intensity increases from a low level— at its equatorward boundary position of ~57° at 2200 local time—to a higher level within the auroral oval. A high level of irregularity intensity exists over the corrected geomagnetic pole. The data base for quantitative measurements at latitudes poleward of the auroral oval, however, is small. On the dayside, the scintillation boundary is in the region of 70° for quiet to moderate magnetic conditions.

During all hours an increase in magnetic activity brings on deeper fading across the entire high latitude region, from the equatorward scintillation boundary to the geomagnetic pole.

Precipitation of electrons, with energies of the order of a few hundred eV, is not thought to be the mechanism for the production of small scale irregularities. In this energy range, electron precipitation shows a low occurrence in the polar cavity while scintillations remain high in this region.

Measurements of suprathermal electrons show polar patterns closer to the scintillation observations than measurements of high energy electrons. Irregularities observed in thermal-electron satellite observations (R. Sagalyn, private

2

communication, 1973) at high latitudes—including polar areas—show geomagnetic
occurrence patterns—together with those in polar areas—similar to the ones shown
in this paper. In their measurements of turbulent isotropic electric fields at
400 km, Kelley and Mozer (1972) have found variations with latitude in the boundary
region, the auroral oval and over the pole which resemble those postulated in this
model.

1.1 INTRODUCTION

At high latitudes, small scale (1 to 10 km) field-aligned irregularities in the
F layer have been detected by many techniques. These include bottom and topside
sounders, scintillation recordings of radio stars and satellite beacons, and in situ
Langmuir probes and vector electric field detectors.

The model of high-latitude irregularity morphology to be presented stems
from a critical evaluation of published and new material on scintillations. The
sketch of the model takes its form from the detection technique employed. In this
case, the perspective is dictated by data available from diffraction observations of
radio signals as they traverse the ionospheric holes or enhancements.

Other views of the irregularity scene have emerged using different perspectives.
Spread F measurements, made by ground ionosounders, are severely limited at
high latitudes by strong absorption during proton events and during periods of
auroral absorption. In addition, spread F returns are screened by E-layer auroral
reflections and by sporadic E. Topside soundings display only those F-layer ir-
regularities above the peak of the F layer. In commonly available observations of
both topside and bottomside soundings, only occurrence or non-occurrence of
spread F is available; quantitative values are not given.

Scintillation data is quantitative in its scaling. New analyses (Whitney et al,
1972) have allowed frequency dependence scaling to be performed. The combina-
tion of radio star observations, low-altitude (1000 km) satellite transmissions, and
synchronous satellite observations had produced a mix of elevation angles, snap-
shots of the irregularity structure, and long-term synoptic measurements which
can be assembled into a model.

In addition to irregularities produced at high latitudes by processes related
to magnetospheric causation, other types of irregularities at both E and F layers
produce scintillations. These include isolated F-layer patches (Slack, 1972) and
sporadic E of the spread type (Anastassiadis et al, 1970 and Chen et al, 1972).
These can be of importance at latitudes in the region of 55° or lower, but their
occurrence pattern and the magnitude of their effect on signals in the 100 MHz
range and higher is less than the effect of magnetospherically-associated, high-
latitude irregularities in the auroral and polar cap regions.

In this paper, one will notice that a large percentage of the observations being used consists of data from the observatories associated with the author. The rationale is that the data have been analyzed in consistent quantitative terms, are available for statistical manipulation, and fall along a relatively narrow longitudinal swath (51° to 71° West, except for a small amount of data from Alaska).

The records were reduced by the method given by Whitney et al (1969) into 15-min scintillation indices. In this system, a scintillation index of 40 represents a +1.5 dB to -2.2 dB excursion from mean quiet level; an index of 60 represents +2 dB to -4 dB.

Figure 1.1 is an outline of the general form of the irregularity region during periods of very quiet magnetic activity, Kp = 0, 1, and for one disturbed magnetic
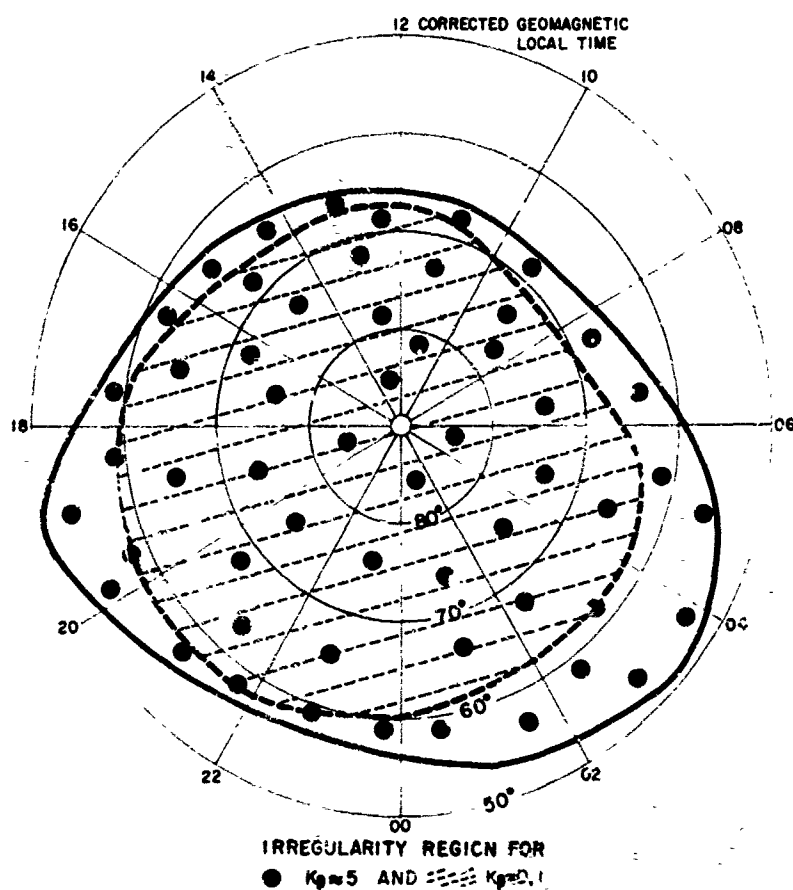

IRREGULARITY REGION FOR
● Kp≈5 AND ----- Kp=0,1

Figure 1.1. Diurnal Pattern of the Extent of the F-Layer Irregularity Region During Quiet Magnetic Conditions (Kp = 0, 1) and for Kp ≈ 5

index, (Kp ≈ 5) (in the text that follows, index K only is used). This paper will describe the variations of the boundary of the irregularity region, the change of intensity of the irregularities within the region, and the occurrence of irregularities within the polar cap. We have assumed that the irregularities are at F-layer heights; the work of Lizka (1964) and Frihagen (1969), as well as others, has established the region between 250 and 500 km as the predominant height range for the irregularities that produce scintillations.

1.2 THE LOWER BOUNDARY

1.2.1 Night Observations

1.2.1.1 MAGNETICALLY QUIET CONDITIONS

By statistically analyzing observations of Transit 4A scintillations at 54 MHz, it was determined (Aarons et al, 1969) that the scintillation boundary had an oval form, differing substantially in both latitudinal peregrinations and precise positions from the optically derived E-layer auroral oval. The boundary falls to 57° invariant latitude at 2200 local time for K = 0, 1; the auroral oval has a lower boundary of 60° for the same magnetic conditions (Feldstein and Starkov, 1967). The definition of the lower latitude of the irregularity region, termed the scintillation boundary, was arbitrary in one sense; that is, it was chosen as the latitude at which the mean scintillation index at 40 MHz reached or exceeded 50 percent. It corresponded, however, to the latitude where the sudden onset of irregularities was observed. In that sense, it is the boundary between the ordered F layer and the irregularity region.

Recent papers have broadly verified the midnight boundary position. Oksman and Tauriainen (1971) found a boundary latitude of 59° for K ≤ 3 shortly after midnight. Kersley et al (private communication, 1971) found a scintillation boundary of 54° shortly before midnight for K = 0, 1. Kaiser and Preddey (1968) found somewhat lower transition latitudes around midnight in the southern hemisphere.

It should be stressed that the irregularity region's equatorward boundary is statistical. It may move to latitudes higher than those shown in Figure 1.1 for K = 0, 1. When the K index remains consistently low over a period of days, Aarons et al (1972) have shown that the midnight boundary may retreat to latitudes higher than 64°.

In Figure 1.2, the mean scintillation index at 136 MHz is plotted as a function of invariant latitude for the broad local time period 2200-0200, and for quiet (0, 1), moderate (2, 3), and disturbed (4-9) conditions. The genesis of this diagram will be outlined as individual time periods and magnetic conditions are examined.

For K = 0, 1 the irregularity region starts abruptly at 60^{c} with an index of ~8 percent (which corresponds to an index of 50 at 40 MHz). The intensity of the irregularities

Figure 1.2. Idealized Curves of the Variations With Latitude of
Mean Scintillation Index at 136 MHz as a Function of Kp. The values
are given for the local time period of 2200-0200

increases with latitude up to 66°, remaining constant until 73°, decreasing slightly
in a trough region but increasing over the pole to a value slightly below its auroral
oval level. We have used broad dashes above 80° to indicate the uncertainty in
values due to the sparcity of data for this region.

A great deal of data is available for the latitudinal region 50° to 64°, somewhat
less for the region 54° to 82°, and very little for the region 82° to the pole. Night
measurements in the lower portion of the irregularity region are plentiful, due to
the high occurrence of observatories at middle and auroral latitudes.

1.2.1.2 MAGNETICALLY DISTURBED CONDITIONS

When magnetic conditions become disturbed, two effects can be noted (see
Figure 1.2):

(1) Boundary Motion: During periods of magnetic disturbance, the boundary of
the irregularity region drops to lower latitudes. Aarons and Allen (1971) have
shown that the maximum change—2 to 2.5°/K—in the nighttime equatorward bound-
ary, as a function of K index, took place between 0200 and 0600 local time. The
nightly mean was a 1°/K lowering of the boundary latitude.

(2) Increase in Index: Mean scintillation index increases throughout the entire
auroral and polar region during periods of magnetic disturbance, although the per-
centage of increase may vary as a function of latitude. From the evidence of scintil-
lation measurements, there is no indication of a polar cavity in the occurrence of
deep scintillation at any time.

In the region between the boundary and below the quiet auroral oval, the depth of scintillation was deteimined by comparisons of many measurements; these included zenithal observations of Cassiopeia at 113 MHz (Aarons and Allen, 1966), and a comparison study of satellite beacon and radio star measurements (Basu et al, 1964).

1.2.2 Day Observations

Through a recent analysis of observations of the 40 MHz transmissions of BE-B taken at Narssarssuaq, Greenland in collaboration with the Danish Meteorological Institute, we have been able to revise the daytime boundary; the revision is incorporated in Figure 1.1. Narssarssuaq, at an invariant latitude of 69° (at 350 km) allowed the daytime boundary to be defined for K = 0,1 and K = 2,3. The boundary and polar indices at 40 MHz are shown in Figure 1.3 for the noon sector. For this time period, the boundary was between 71° and 76^c for K = 0,1 and 68° to 69° for K = 2,3. It was difficult to determine the precise latitude for the lower K indices since the mean SI showed a plateau for the 71° to 76° range. At K = 2,3 the indices rose decisively with latitude and a boundary can be given. From Figure 1.1, it can be seen that the highest equatorward latitude of the irregularity region occurs before noon; there is a distinct assymetry around noon.

In the local time period, 0600-1800, there is a motion of the boundary of approximately $0.5^\circ/K$. The method of analysis for this data was similar to that used in Aarons and Allen (1971). In the noon sector, the auroral oval's equatorward
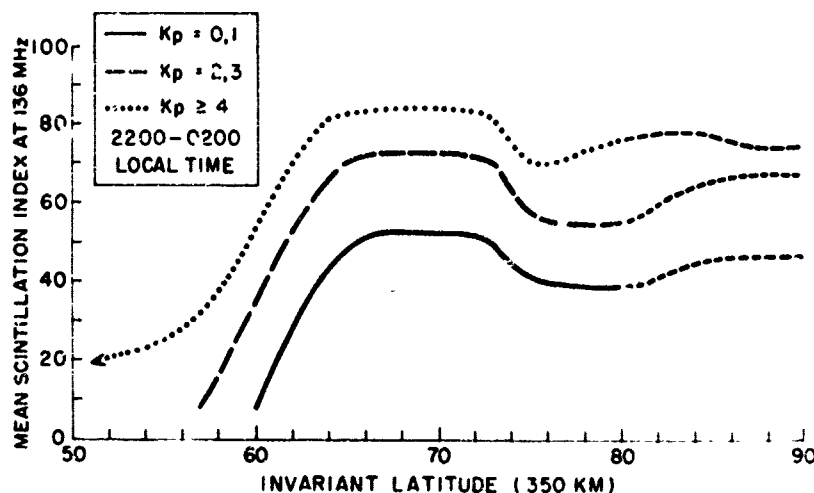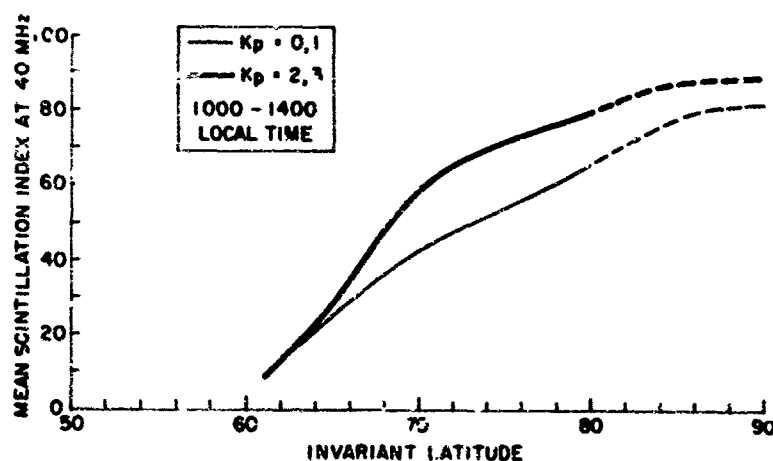

Figure 1.3. Idealized Curves of the Variations With Latitude of Mean Scintillation Index at 40 MHz as a Function of Kp for the 1000-1400 Local Time Period

boundary is 76° at Q (polar range index) = 0 and 69° for Q = 2; this is a close approximation to scintillation observations.

1.3 THE AURORAL OVAL AND THE POLAR CAP

1.3.1 Night Observations

In the midnight sector for Q = 0, the oval extends from 70° to 72° (Feldstein and Starkov, 1967); for Q = 2, the oval extends from 67° to 70°. Scintillation indices appear to maximize broadly in these regions during periods of magnetic quiet.

Much of the data used to construct the curves in Figure 1.2 comes from ground measurements of the scintillations of various synchronous satellite transmissions at 136 MHz. A schematic drawing of the ground station angles of elevation and intersection latitudes is shown in Figure 1.4. Subionospheric latitudes of 54°, 58°, 60°, and 64° were probed and their data used in this paper. Thule observations at a very low angle of elevation (4°) could not be used quantitatively.

Figure 1.5 compares mean scintillation indices for Sagamore Hill and Narssarssuaq for the same days for K = 2, 3, 137 to 223 points for each hour were used.

Another series of data was available for comparison, but only for the period November 1971 to March 1972 (inclusive). This series for Goose Bay, Canada, College, Alaska, and Narssarssuaq, Greenland showed that from 58° to 63°, the change in mean scintillation index—during periods of magnetic quiet—was approximately a factor of 2 for a 2.5° interval. The data for the three stations is shown in Figure 1.6(a) for K = 2, 3 and Figure 1.6(b) for K = 0, 1.

At 66°, a comparison between quiet and moderately disturbed conditions was made using lower transit measurements of the scintillations of Cassiopeia A made at Sagamore Hill with a 150' parabola. The geometry of these measurements, as well as the geometry of upper transit measurements, is shown in Figure 1.7. For one year, June 1963 to June 1964, observations of scintillations of Cassiopeia A were made at 113 MHz and 228 MHz. This data allowed us to compare two sets of magnetic indices for one intersection latitude, 66°. The 113 MHz data are shown in Figure 1.8. Clearly, at 66° there is an increase in scintillation index when magnetic index increases. Upper transit data taken at Sagamore Hill and reported in Aarons and Allen (1966) were also used in the construction of Figure 1.2. In both uses of radio star data, the ratios of scintillation indices were used rather than absolute values.

An extensive series of measurements is available at 64° from Narssarssuaq. This data divided into magnetic index sets of K = 0, 1, K = 2, 3, and K = 4-9
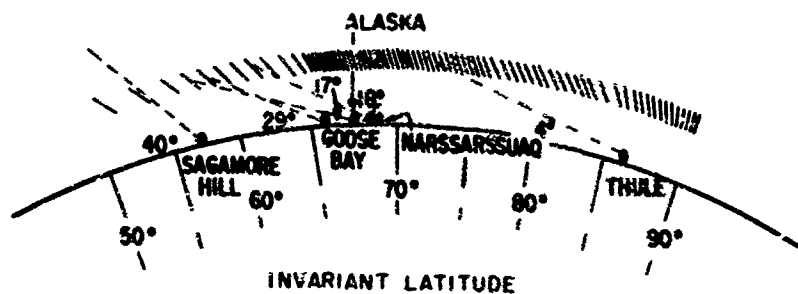
Figure 1.4. Positions of Sites, Intersection Latitudes and Angles of Elevation (for Invariant Latitudes Taken at 350 km) for Observatories Supplying Synchronous Satellite Data Used in This Paper
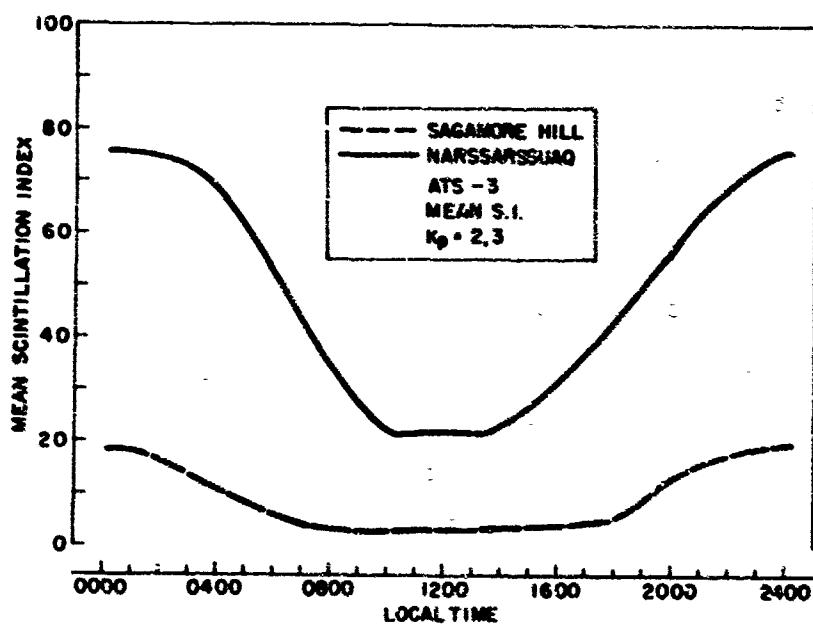
Figure 1.5. Comparison of Mean Scintillation Indices for the Same Hours for Sagamore Hill and Narssarssuaq With Kp = 2, 3
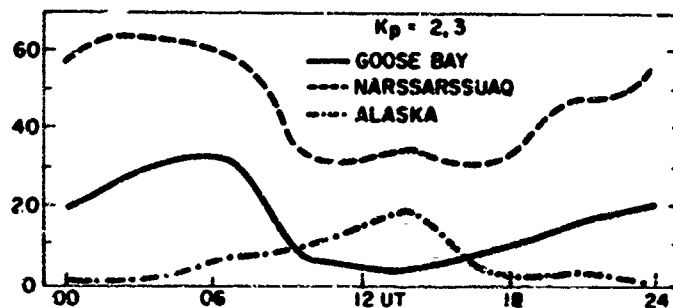
Figure 1. 6a. K Indices of 2, 3 Yield Higher Values of Scintilla-
tion Indices for Both Alaska and Narssarssuaq but Little Change
for Goose Bay Observations
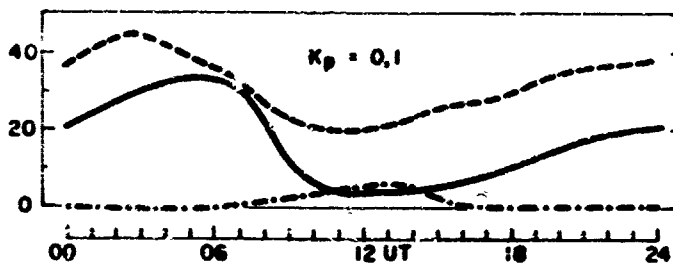
Figure 1. 6b. Mean Scintillation Indices for the Same Time
Period (November 1971 to March 1972) for Three Stations
Situated at High Latitudes. Observations at low K indices (0, 1)
are given in this figure
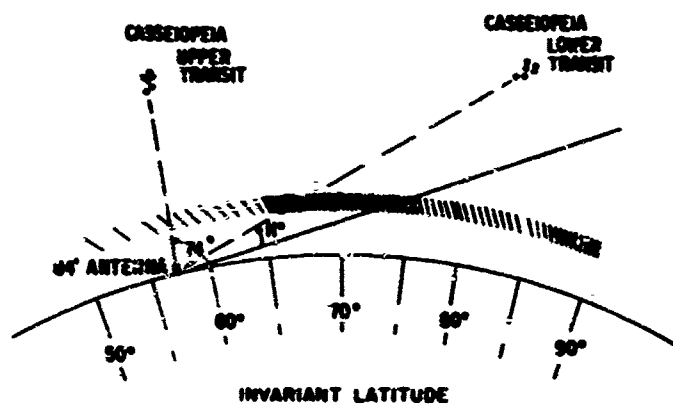
Figure 1. 7. The Geometry of Radio Star Scintillation Measure-
ments From Sagamore Hill is Shown. Data from both an 84 ft
antenna and a 150 ft antenna were used in this paper
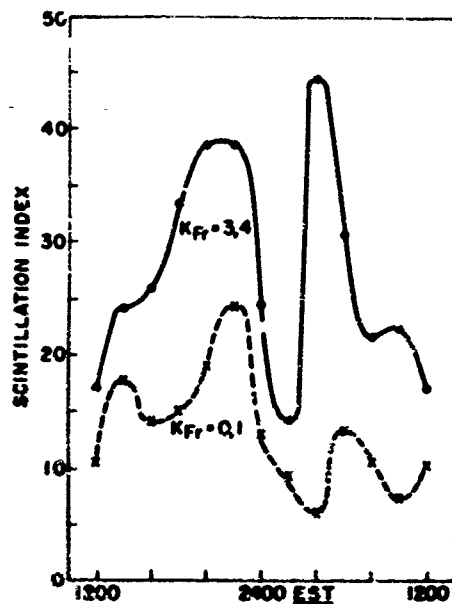
Figure 1.8. Scintillation Indices for 113 MHz
Radio Emission From Cassiopeia A. A 150 ft
antenna at Sagamore Hill was used to make obser-
vations near lower transit (~ 13° of elevation) on a
path intersecting the invariant latitude of 66°
(at 350 km)
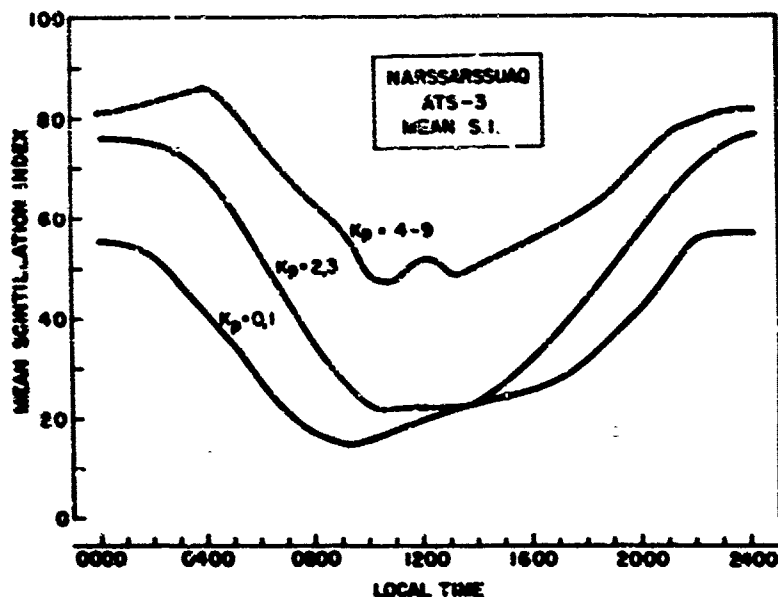
Figure 1.9. Mean Scintillation Indices Recorded at Narssarssuaq, Green-
land as a Function of Local Time and K Index. Note both increasing index
with increasing K index as well as a shift in time of maximum (towards
later local times) with increasing K index

(see Figure 1.9). The difference between the mean values of radio star a d satellite indices is believed to be due to the fact that the radio star data was taken near the minimum in the sunspot cycle, where the satellite data are near maximum. Figure 1.2, therefore, represents sunspot maximum variations with latitude.

1.3.2 Noon Observations

1.3.2.1 MAGNETICALLY QUIET CONDITIONS (K = 0, 1; K = 2, 3)

To construct Figure 1.3, we freely transferred scintillation indices of various types from three sets of high latitude observations. Since the noon boundary begins near 70°, only sites somewhat below this latitude and inside the day portion of the oval and polar cap were useful. Data from the three sites were combined. The sites were Narssarssuaq at 59°, Spitzbergen at 76°, and Thule at 86°. The satellite signal for the three observational sets was the BE-B transmitting at 40 MHz. The scale, therefore, for Figure 1.3 is mean SI at 40 MHz. Since simultaneous high latitude measurements at 40 MHz and 136 MHz signals are available, it is difficult to develop a correction factor.

Equatorward slopes of the curves in Figure 1.3 were obtained from an analysis of the Narssarssuaq data as well as those published by Frihagen (1971), with the latter being taken at Spitzbergen.

At Narssarssuaq, a limited series of measurements of the 136 MHz beacon of the ITOS satellite (orbiting at ~1000 km altitude), were reduced. A steep rise was noted during the noon hours at subionospheric paths north of Narssarssuaq (71° to 72°), corroborating qualitatively the more extensive BE-B measurements.

In a series of measurements at 40 MHz from the polar station, Thule, Nielsen and Aarons (unpublished data, 1973) show a rise at all times of the occurrence of deep fading as the Corrected Geomagnetic Pole is approached.

1.3.2.2 MAGNETICALLY DISTURBED CONDITIONS

During the magnetic storms, both Frihagen (1971) and Nielsen and Aarons (1973) found increased scintillation indices. In the noon sector for $K \geq 3$, Frihagen characterized the scintillations with an index of 4, his highest contour for the latitudinal range 68° to 82°. At noon, comparing disturbed (K = 4-9) and quiet conditions, Nielsen and Aarons found an increase in occurrence of deep fading by a factor greater than 2 from 82° to 83°, but a smaller increase from 88° to 90°.

1.4 ASPECT SENSITIVITY

Two of the principal factors affecting the scintillation index for a particular observatory are aspect sensitivity and angle of elevation. The maximum effect of

a field-aligned irregularity takes place when the line of sight to the radio source and the alignment of the irregularity in the earth's magnetic field are the same (Singleton, 1970). The effect of aspect sensitivity is a function of the propagation angle and th. irregularity characteristics (height, dimensions). Angle of elevation corrections are outlined by Briggs and Parkin (1963); a correction for angle of elevation for large azimuth angles has been inserted for satellites orbiting at low altitudes (1000 km). No correction, however, was introduced for aspect sensitivity in any of the synchronous satellite data or low-altitude satellite data. Many of the observations of the synchronous satellites were compared for magnetic index sets at one site; the aspect angle did not change. In other cases (Narssarssuaq observations, for example), the angle was large (124°) [at 180° the ray path and the irregularity are in line] and, therefore, the amplitude is relatively unaffected.

In the case of a site such as Sagamore Hill and observations of either BE-B or Transit 4A, the manner of lumping data along a line of constant latitude (at various aspect angles) has minimized the effect; the dominant term is a latitudinal variation.

In the case of observations of BE-B from Narssarssuaq and at all times from Thule, aspect sensitivity could be an important factor. Since the minimum propagation angle occurs when the line of sight to the satellite is along the lines of force of the earth's field, in the case of Narssarssuaq and Thule data it is to be expected that minimum index would occur along the magnetic meridian and to the south of the station. At noon from Narssarssuaq (Nielsen and Aarons, 1973), maximum index occurred to the north of the observatory. At all times at Thule, scintillation index occurrence was maximum to the north of Thule in the direction of the corrected geomagnetic pole. A correction, however, should be made to absolute values but the indices given in this paper in the polar cap region are hardly in that category.

It might be noted that in an analysis of 40 MHz data from BE-B taken in southern polar regions, Titheridge and Stu... (1968) found a high level of activity over a region between the southern geographic pole and the geomagnetic pole. From a position almost equidistant from the geographic, they observed the geomagnetic and the dip poles. A similar lumping together of the data supplied by Mullen and Buerkle (private communication, 1971) of the scintillations of the 150 MHz transmissions from the Transit satellite is shown in Figure 1.10. K indices were limited to 0-2. Maximum scintillation occurrence is near the vicinity of the corrected geomagnetic pole; this is considerably higher than the Foxe Basin maximum found by Penndorf (1962) in his bottomside-spread F analysis. Thus it can be seen that aspect sensitivity cannot account for the polar maximum near the geomagnetic pole.
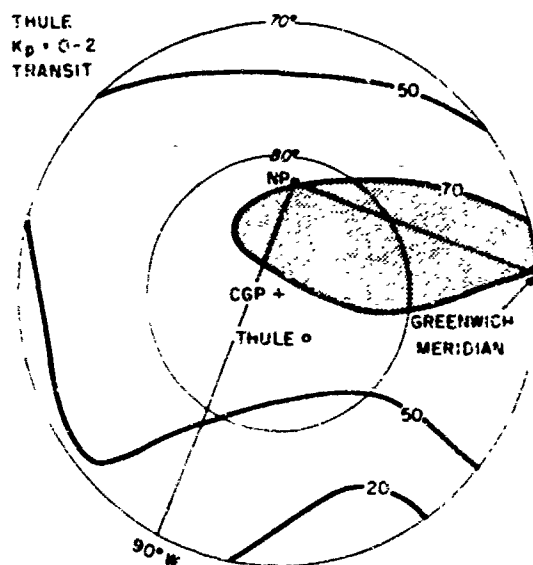
Figure 1.10. Occurence of Scintillations (Arbitrary on-off Determination) at 150 MHz From the Transit Satellite Observed at Thule for Kp = 0-2. All times of day are included in this series of observations during the summer of 1968. Data from Mullen and Buerkle (private communication)

1.5 DISCUSSION

The morphology and latitudinal variations of F-layer irregularities—as shown by scintillation observations—set limitations to proposed mechanisms for the origin of the irregularities.

Low energy electrons, from 1 to 1000 eV, precipitating into the ionosphere will produce ionization at F-layer heights (Frihagen, 1969). The polar boundary observed for precipitation of electrons of a few hundred electron volts negates the concept that these electrons are sources for production of irregularities. In reviewing high latitude observations of low-energy particle precipitation, O'Brien (1970) found that fluxes in the polar cap (defined for his study as 74° to 84° during local day and 71° to 83° during local night) were 10 to 1000 times less than in the soft zone. Hoffman (1970) found the polar cavity appearing as a region of no measureable precipitation (with the detectors used). Yet all available data between 75° and the pole (Frihagen, 1971; Titheridge and Stuart, 1968; Nielsen and Aarons, 1973) show that a high occurrence of scintillation prevails throughout this region. Maier and Rao (1970), observing suprathermal electrons (> 5 eV), discuss a poleward boundary higher than the auroral oval. In their graphs, they show less difference between auroral oval flux and polar flux for suprathermal electrons than for the higher energy electrons. R. Sagalyn (private communication, 1973) observing thermal positive ion flux over high latitudes, most often failed to find a poleward boundary for the irregularities observed.

Another possible mechanism is the generation of instabilities at F-layer heights by the precipitation of low energy electrons. The wave motion might then flow polew .. and equator ard. An important characteristic of scintillation, how-ever, is its great variability within spans of tens to hundreds of kilometers. It would be reasonable to expect waves generated at nigh latitudes in relatively small east-west regions to spread out uniformly at lower latitudes over larger east-west areas. Scintillation characteristics, as shown in Basu et al (1964), show con-siderable differences between neighboring geographical areas. In addition, it is difficult to account for the stopping of a wave motion abruptly at the scintillation boundary. One characteristic of scintillation—the decrease in irregularity intensity from the auroral oval to the boundary—would, however, fit in with an attenuation of a wave generated in the auroral oval.

The characteristics of scintillation in the irregularity region point to another possible mechanism; that is, the disturbance of field lines. In their measurements of electric fields at 400 km, Kelley and Mozer (1972) have found variations with latitude in the boundary region, the auroral oval, and the polar regions which resemble those record ed in scintillation studies. Maximum signals of a turbulent isotropic electric field were found in regions of invariant latitude corresponding to the average position of the oval. High intensities were also found in polar regions. Day values decreased significantly over the geomagnetic pole relative to auroral oval levels in their spring measurements. One the hypotheses, advanced by Kelley and Mozer, is that the signals they detect with their experiment are due to electrostatic oscillations established independently on neighboring field lines. This hypothesis would satisfy the observations of localized variations, as well as the need to introduce an explanation of the polar observations of a high occurrence of deep fading.

Although the "tweaking" of magnetic field lines both in the closed and open field lines appears to satisfy observational demands, it hardly explains what produces the change in conductivity along the field lines from closed field lines right into the tail.

1.6 SUMMARY

The outlines of the intensity variations within the irregularity region are clear. At night during periods of magnetic quiet, scintillation index increases several.old from the boundary to the auroral oval latitudes. Maximum index is recorded in the auroral oval region. A shallow minimum is then encountered with a second peak located near the corrected geomagnetic pole. Higher magnetic indices both increase intensity levels across the entire irregularity region, and

lower the boundary between the ordered F layer and the F layer encrusted with small scale irregularities.

The daytime boundary is located between 71° and 76° for very low K indices (K = 0, 1) and $68-66^\circ$ for K = 2, 3. Increased magnetic activity brings higher levels of scintillations throughout the region from the boundary to the corrected geomagnetic pole during the day, as well as during the night.

Low energy electrons would precipitate at F-layer heights. The normal absence from the polar regions (the polar cavity) of a high flux of electrons greater than several hundred eV, however, makes it difficult to ascribe F-layer irregularities directly to precipitation of electrons within this energy range. Suprathermal electrons (> 5 eV) and thermal electron irregularity patterns, however, show occurrence similar to those of scintillation indices. An association—which is very close from the point of view of latitude of occurrence, variation with magnetic index, and polar pattern—is that of electric field turbulence. One of the two possible reasons for the presence of the isotropic turbulent electric fields put forth by Kelley and Mozer (1972)—that is, the change in conductivity along individual field lines—is thought reasonable from the viewpoint that scintillation characteristics with their strongly localized intensity variations demand localized field line variations.

References

Aarons, J. and Allen, R.S. (1966) Scintillation of a radio star at a subauroral latitude, Radio Science 1:1180-1186.

Aarons, J. and Allen, R.S. (1971) Scintillation boundary during quiet and disturbed magnetic conditions, J. Geophys. Res. 76:170-177.

Aarons, J., Mullen, J.P. and Whitney, H.E. (1969) The scintillation boundary, J. Geophys. Res. 74:884-889.

Aarons, J., Whitney, H.E., and Allen, R.S. (1971) Global morphology of ionospheric scintillations, Proc. IEEE 59:159-172.

Anastassiadis, M., Matsoukas, D., and Moraitis, G. (1970) 40-MHz ionospheric scintillation and the sporadic E layer, Radio Science 5:953-957.

Basu, S., Allen, R.S. and Aarons, J. (1964) A detailed study of a brief period of radio star and satellite scintillations, J. Atmos. Terr. Phys. 26:811-823.

Briggs, B.H. and Parkin, I.A. (1963) On the variation of radio star and satellite scintillations with zenith angle, J. Atmos. Terr. Phys. 25:339-350.

Chen, A.A., Chin, P.N. and Chance, M.P. (1972) Field-line connection between scintillation and ionospheric conditions causing spread E, J. Geophys. Res. 77: 1859-1863.

Feldstein, Y.I. and Starkov, G.V. (1967) Dynamics of auroral belt and polar geomagnetic disturbances, Planet. Space Sci. 15:209-229.

Frihagen, J. (1969) Satellite scintillation at high latitudes and its possible relation to precipitation of soft particles, J. Atmos. Terr. Phys. 31:81-92.

Frihagen, J. (1971) Occurrence of high latitude ionospheric irregularities giving rise to satellite scintillation, J. Atmos. Terr. Phys. 33:21-30.

Hoffman, R.A. (1970) OGO-4 satellite measurements of low energy - high latitude electron precipitation, in The Polar Ionosphere and Magnetospheric Processes, edited by G. Skovli, p. 79-91, Gordon and Breach, New York.

Kaiser, ..B. and Preddey, G.F. (1968) Observations of transitions in satellite scintillation, J. Atmos. Terr. Phys. 30:285-291.

Kelley, M.C. and Mozer, F.S. (1972) A satellite survey of vector electric fields in the ionosphere at frequencies of 10 to 500 Hz, 1. Isotropic, high latitude electrostatic emissions, J. Geophys. Res. 77:4158-4173.

Liszka, L. (1964) An investigation of the height of scintillation producing irregularities, Arkiv Geofysik 4 :523.

Maier, E.J. and Narasinga Rao, B.C. (1970) Observations of the suprathermal electron flux and the electron temperature at high latitudes, J. Geophys. Res. 75:7168-7174.

O'Brien, B.J. (1970) Low energy particle fluxes over the polar cap, in The Polar Ionosphere and Magnetospheric Processes, edited by G. Skovli, p. 49-66, Gordon and Breach, New York.

Oksman, J. and Tauriainen, A. (1971) On annual movements of the scintillation boundary of satellite signals, J. Atmos. Terr. Phys. 33:1727-1735.

Penndorf, R. (1967) Geographic distribution of spread F in the Arctic, J. Geophys. Res. 67:2279-2288.

Singleton, D.G. (1970) The effect of irregularity shape on radio star and satellite scintillations, J. Atmos. Terr. Phys. 32:315-343.

Slack, F.F. (1972) Quasiperiodic scintillation in the ionosphere, J. Atmos. Terr. Phys. 34:927-939.

Titheridge, J.E. and Stuart, G.F. (1968) The distribution of irregularities in the antarctic ionosphere - I. Mean seasonal maps at sunspot minimum, J. Atmos. Terr. Phys. 30:85-98.

Whitney, H.E., Aarons, J. and Malik, C. (1969) A proposed index for measuring ionospheric scintillations, Planet. Space Sci. 17:1069-1073.

Whitney, H.E., Aarons, J., Allen, R.S. and Seemann, D.R. (1972) Estimation of the cumulative amplitude probability distribution function of ionospheric scintillations, Radio Science 7:1095-1104.

Contents

2. A Graphical Description of Scintillation Occurrence Patterns

Jules Aarons
Radio Astronomy Branch
Ionosphere Physics Laboratory
Air Force Cambridge Research Laboratories
Bedford, Massachusetts

2.1 INTRODUCTION

Utilizing observations of ATS-3 at 136-137 MHz, 15-min scintillation indices were scaled from chart records. The observations for the stations were taken over varying periods of time. From the Sagamore Hill Radio Observatory where the mean intersection latitude was $\sim 54^{\circ}$ invariant (elevation angle $\sim 40^{\circ}$), the data encompass the period from November 1967 to March 1972 with some gaps in the reduced data base. From the Narssarssuaq Observatory of the Danish Meteorological Institute, the records were reduced for the period September 1968 to March 1972 (with gaps). The mean intersection latitude was $\sim 64^{\circ}$ with an elevation angle of $\sim 18^{\circ}$. The Thule observations made at the AFCRL Geopole Station, through an intersection latitude of 72° invariant and an elevation angle of $\sim 4^{\circ}$, were reduced for ~ 90 days; it was felt that the wide range of variations and the low angle of elevation limited the utility of the Thule data and therefore the need to reduce more data.

In the graphical (and statistical) analyses, we have utilized seasons to conform approximately with astronomical considerations (February, March, and

April for Spring, etc.). We have subdivided magnetic index into the three groups: Kp = 0, 1, Kp = 2, 3, and Kp = 4-9. We use K throughout the studies shown. In Appendix A, we use K index groups to assist the systems analyst in organizing the data for applicability to different stages of the sunspot cycle.

2.2 THE SAGAMORE HILL RADIO OBSERVATORY

The data for the Sagamore Hill intersection is that applicable to a subauroral position.

The diurnal pattern for each of the four seasons is summarized for all of the data reduced in Figures 2.1(a), (b), and (c) for the magnetic groupings K = 0, 1, K = 2, 3, and K = 4-9.

For K = 0, 1, the occurrence of scintillation indices is somewhat higher in the spring than in the other seasons, with winter showing the lowest maximum to minimum ratio. The same pattern takes place when the K indices are higher (2, 3); that is, maximum occurrence of indices greater than 20 in the spring and smallest diurnal variation during the winter. The seasonal pattern of high spring values continues in Figure 2.1(c) (K indices are 4-9 while the scintillation index is greater than 40 in this case). Winter continues to have a relatively high post-noon level.

Subdividing the data into individual seasons, year by year, the graphs of Figures 2.2(a), (b), (c), and (d) result for K indices of 0, 1. The pattern for each season has some degree of consistency for each of the years shown. Similar graphs for K = 2, 3 are shown in Figures 2.3(a) - (d). The total data bank is used for the K sorts of Figures 2.4(a) and (b).

Using the mean of the occurrence of SI > 20—the two highest hourly values of scintillation index—to characterize individual seasons, Figure 2.5 has been constructed for K = 0-3; the data is inadequate to determine the effect of changing sunspot number. The particular period of time, 1968-1972, had several years of almost identical sunspot number.

2.3 NARSSARSSUAQ, GREENLAND

The seasonal comparison for the Narssarssuaq data is shown in Figures 2.6(a)-(d). The quiet day curves of K = 0, 1 can be noted in Figure 2.6(a). Summer has the highest maximum of occurrence of scintillation indices greater than 60 (the parameter used in most of the curves in this section) with winter showing a very small change diurnally. This pattern of very high occurrence of deep fading at night in the summer (and to a lesser extent in the spring) also

shows up in K indices of 2, 3 [Figure 2.6(b)]. An afternoon maximum is seen in winter with a low occurrence of nighttime scintillations. It might also be noted that summer levels go to zero during early morning hours even when the nightly occurrence is above 90 percent. With magnetic storm conditions, the same diurnal variations hold. In Figure 2.6(c) we continue to use SI > 60, while in Figure 2.6(d) we have plotted SI > 80. It might be noted that minimum occurrence for the 64° latitude intersection occurs before noon for all K indices. A post-noon hump can be noted at high K indices in three seasons: winter, fall, and summer.

The pattern of occurrence for each season for the years with adequate reduced data is shown in Figures 2.7(a) - (d) for K = 0, 1, and Figures 2.8(a) - (d) for K = 2, 3; it is believed that the data were remarkably consistent when the sorts have been performed in the manner shown. The magnetic storm data have too high values and are too sparse to show the pattern of seasonal behavior year by year.

Figure 2.9 utilizes the entire data bank to determine the trend of indices. From Figure 2.9(a), it can be noted that the time of maximum occurrence of SI > 60 shifts towards the latter part of the morning with increasing K index. Figure 2.6(b) shows the diurnal pattern using the occurrence of very high scintillation index of 80 for K = 0-3, and K = 4-9.

To determine the long term trends of the material, Figure 2.10 has been plotted. The mean of the two highest hourly values of percentage of occurrence of SI > 60 has been plotted (K = 0-3). Little can be said about the effect of the sun; only with the oncoming solar minimum can the effect of solar flux be evaluated.

2.1 THULE, GREENLAND

Problems with Thule recordings were considerable. Since the angle of elevation was so low (~4°) and the wave propagation path almost always through the auroral oval (at some height), scintillations at 136 MHz were very high. Figure 2.11 shows Thule SI > 60 for K = 0, 1 and SI > 80 for K = 0-3. A high percentage of occurrence at night can be noted for what is effectively our highest value of scintillation index (SI > 80).
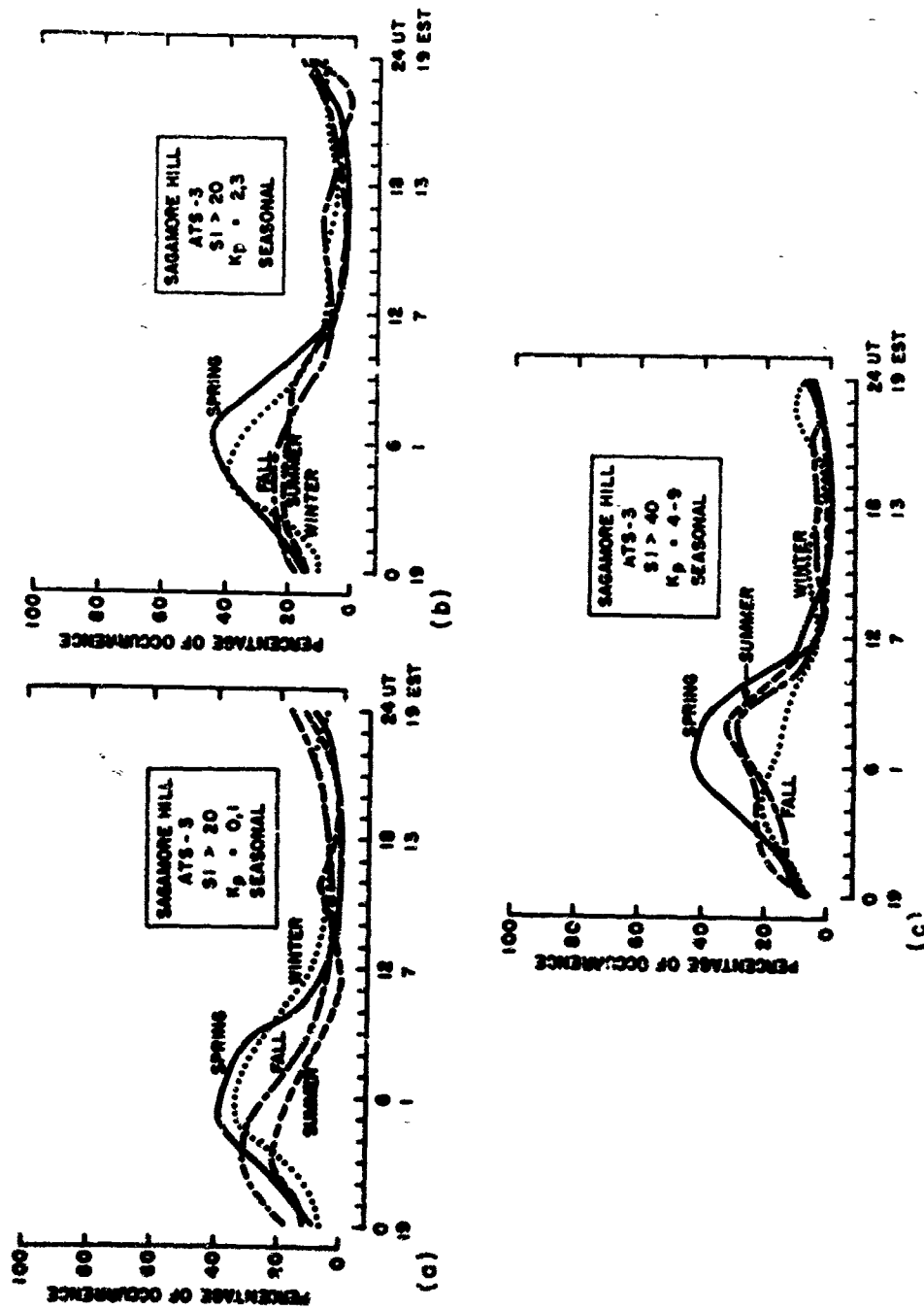
Figure 2.1
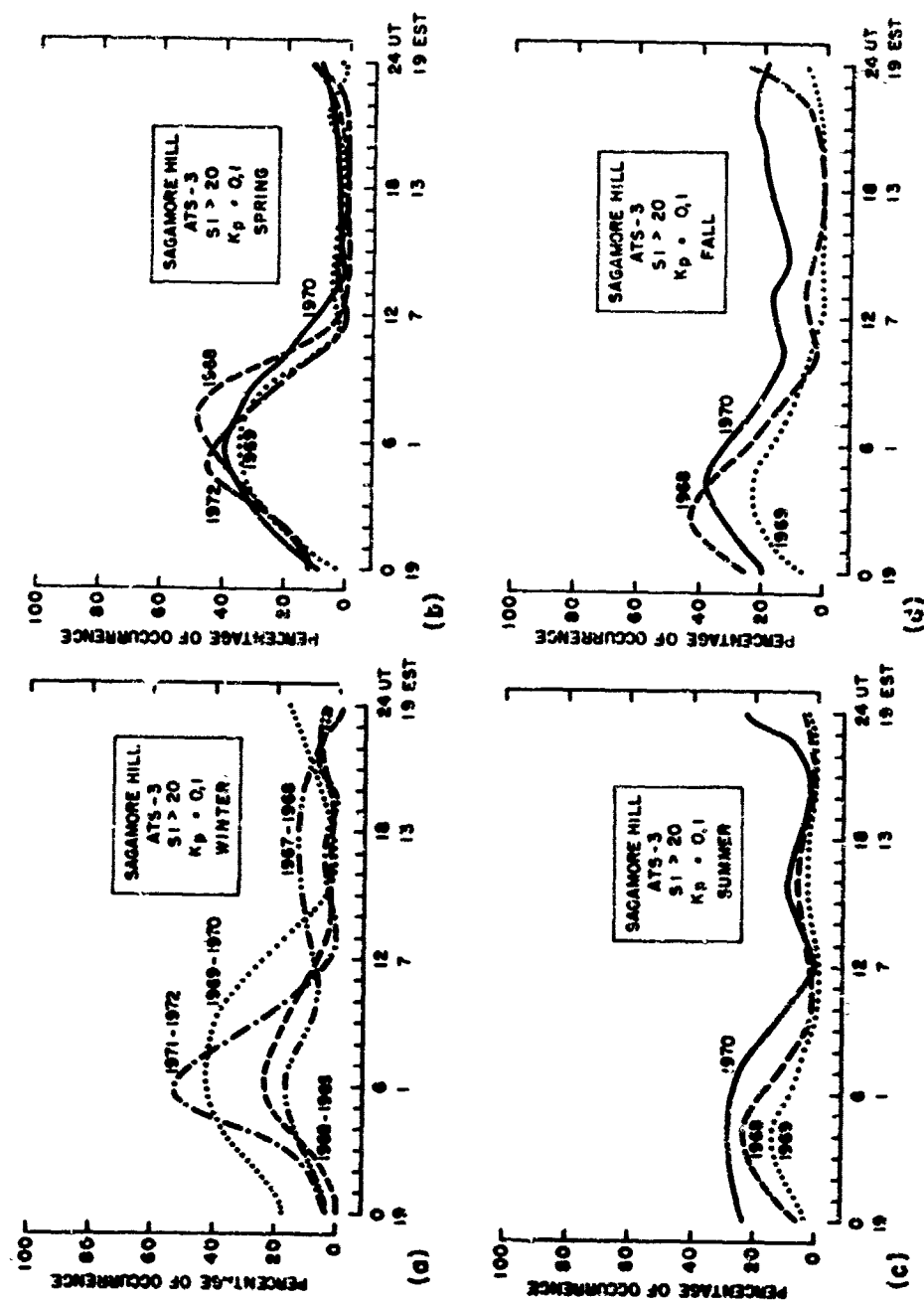
Figure 2.2
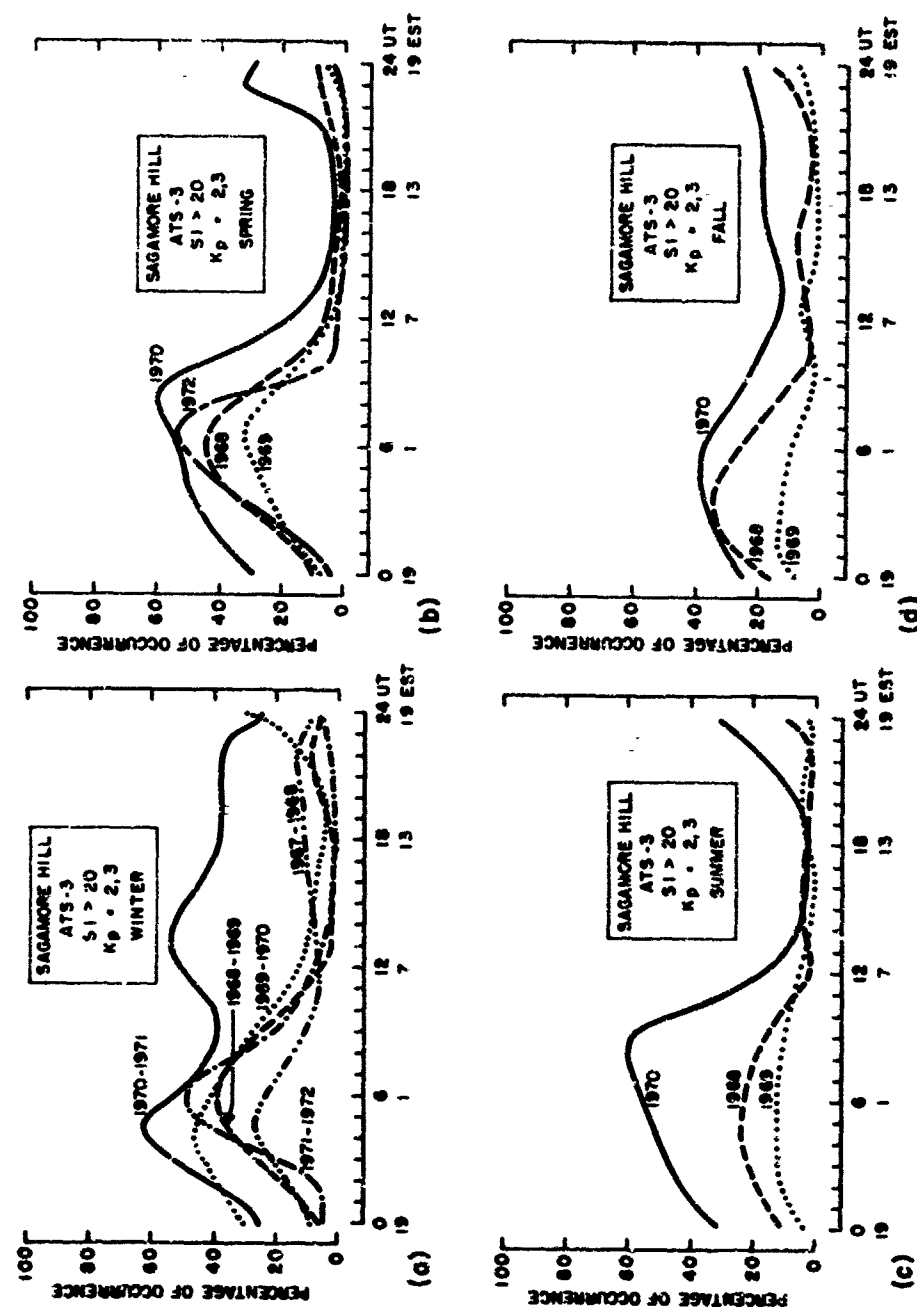
Figure 2.3
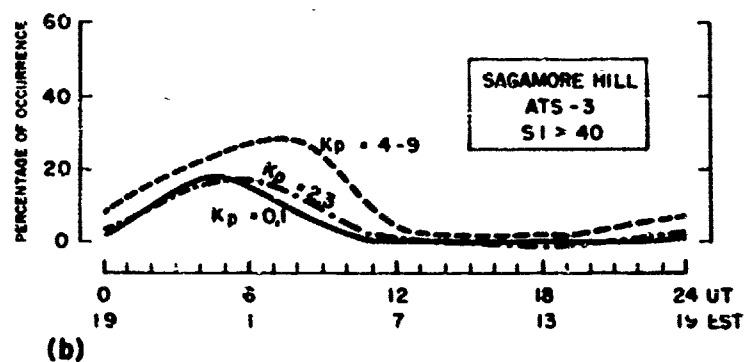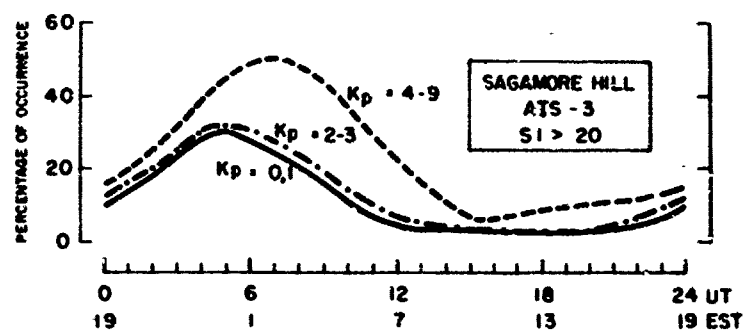
Figure 2.4
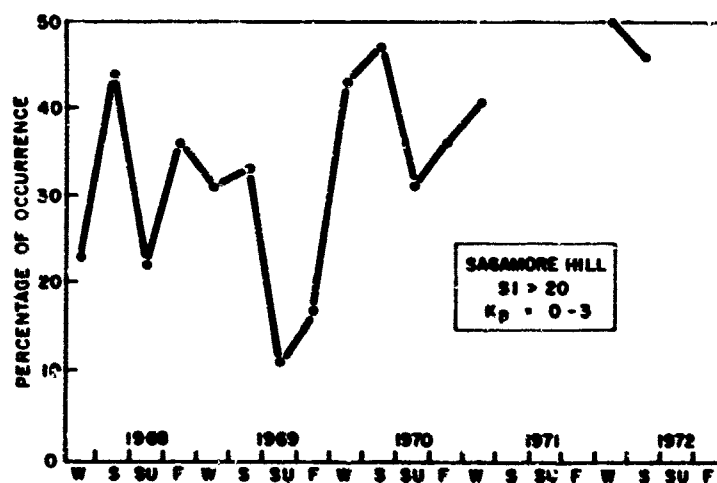
Figure 2.5
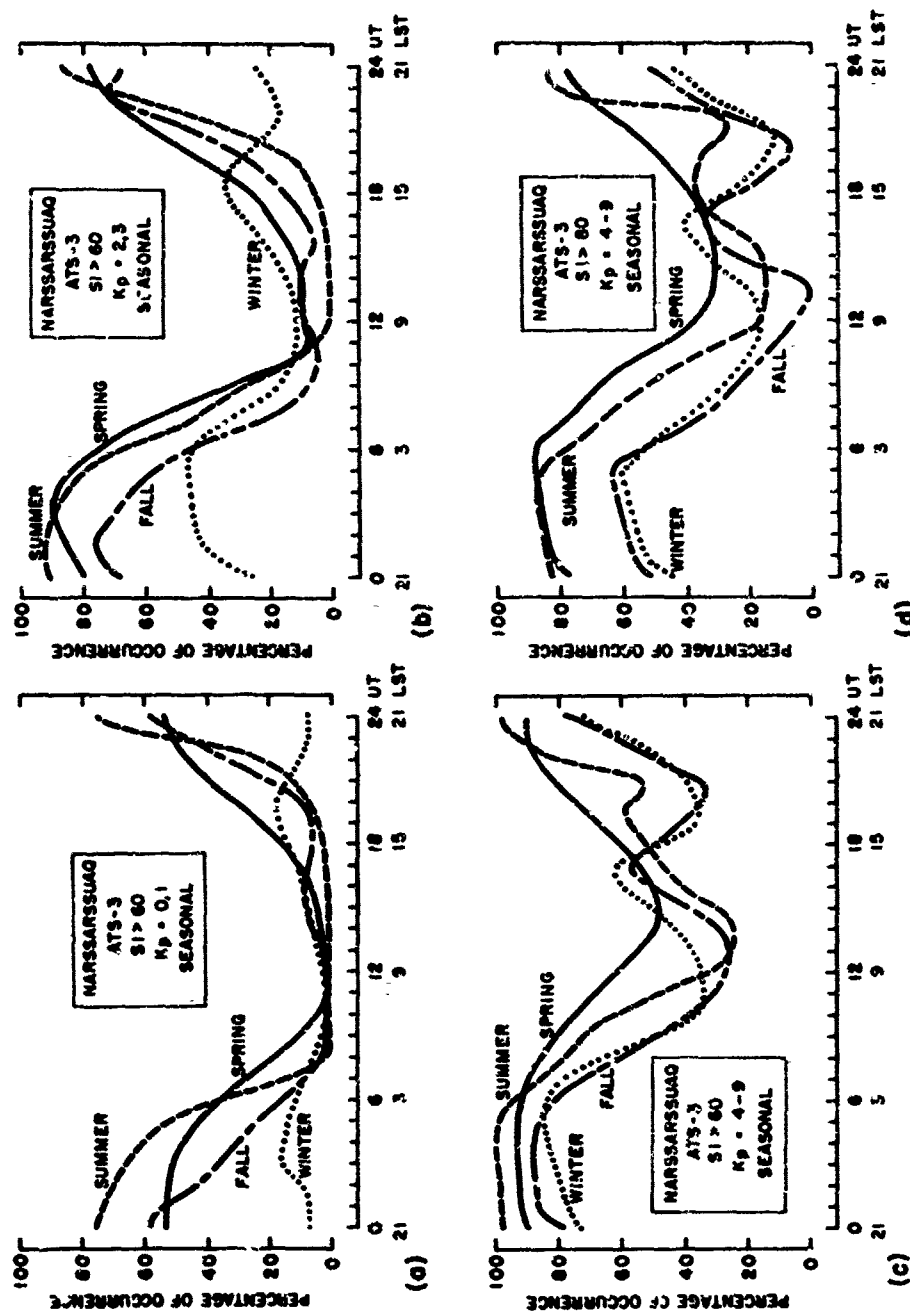
Figure 2.6
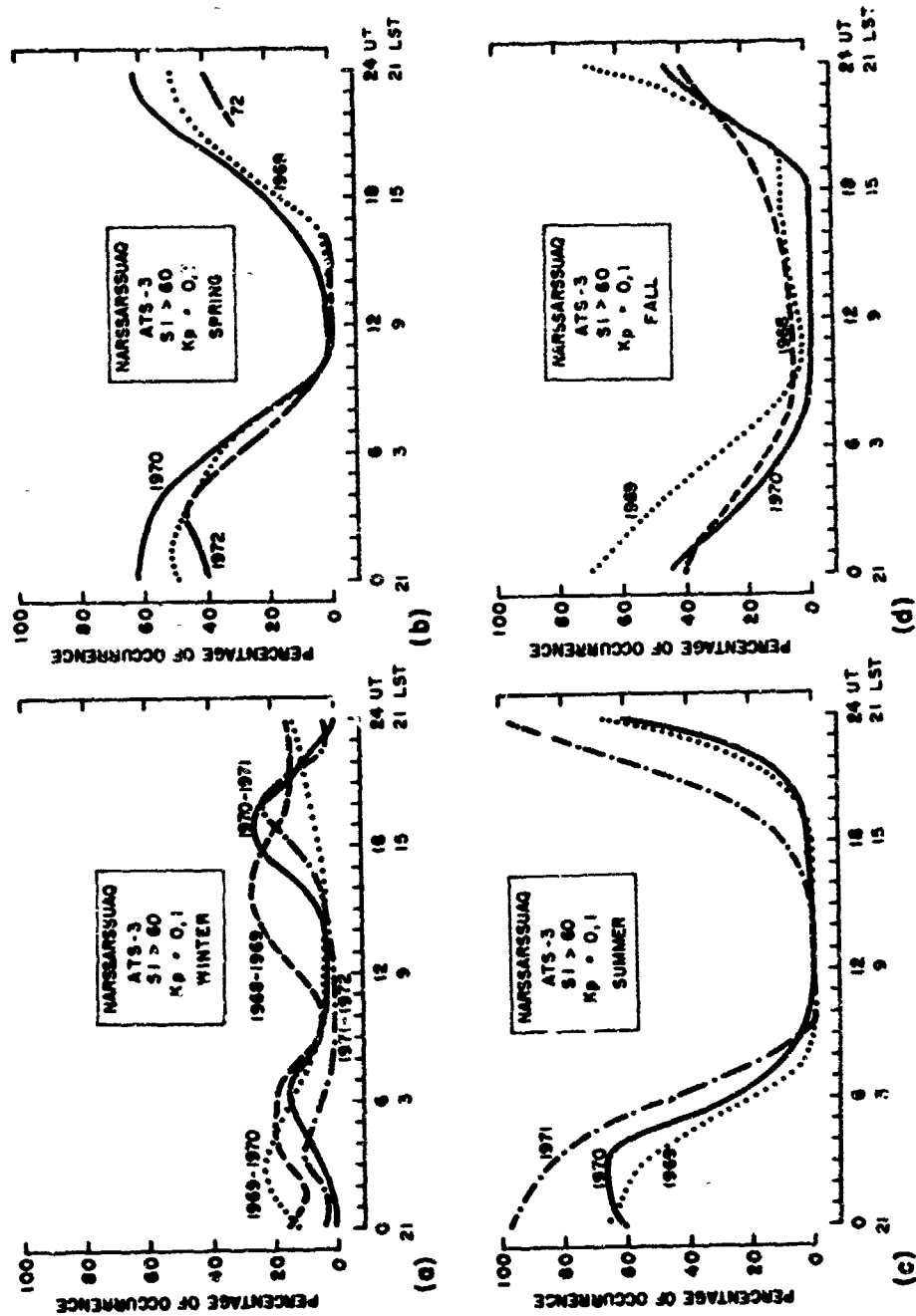
Figure 2.7

Figure 2.8

Figure 2.9

28

Figure 2.10

Figure 2.11

Contents

3. A High Latitude Statistical Model of Scintillations Using the Cumulative Amplitude Probability Distribution Function

Herbert E. Whitney, Richard S. Allen
and Douglas R. Seemann
Radio Astronomy Branch
Ionospheric Physics Laboratory
Air Force Cambridge Research Laboratories
Bedford, Massachusetts

3.1 INTRODUCTION

Various scintillation indices have been used to describe the depth of amplitude scintillations. These indices can be summarized into four types dependent on whether mean or rms value describes the excursions and whether amplitude or power describes the signals. Briggs and Parkin (1963) and Bischoff and Chytil (1969) list and discuss the indices.

At AFCRL, a standard method of measurement was adopted for ionospheric studies (Whitney et al. 1969). The aim of the studies was to describe the morphology of the irregularity structure. Therefore a simple method had to be utilized to reduce the strip charts. The index adopted is defined as:

$$S.I. \ (\%) = \frac{P_{max} - P_{min}}{P_{max} + P_{min}} \times 100 , \tag{3.1}$$

where P_{max} is the third peak down from the maximum and P_{min} is the third minimum up from the lowest excursion in the given sample period. The majority of the data that is to be described was scaled to have one index value which characterized a 15-min interval. The data used is that obtained by observations of various synchronous satellites transmitting at 136 MHz. A 15-min sample interval was chosen in order to achieve stationarity or constancy of scintillation index over the measurement period. In the latitudes just below the auroral oval, scintillations have periods that range from about 1/sec to 1/min with a median value of six fluctuations per minute. The same range of periods holds for the equatorial region, with longer periods observed in the post midnight hours (Aarons et al, 1971). Faster fluctuations are frequently observed at high latitudes, when observing synchronous satellites at low angles of elevation through the auroral oval. Examples of the variation in rate can be seen in the strip chart reproductions in Figure 3.1. A 15-min interval will, therefore, include many periods of the scintillations, while a longer sample interval for the measurement of S.I. would be subject to possible changes in scintillation index from the variability of the propagation path.

3.2 SCINTILLATION INDEX AND PROBABILITY DISTRIBUTIONS

The parameter scintillation index does not describe precisely the fading characteristics of the signal in sufficient detail for either the engineer interested in propagation effects, or for the physicist interested in determining scattering mechanisms for the signal. Engineers designing satellite systems must determine the fading margin necessary to overcome ionospheric scintillations under various conditions—and for a particular electronic configuration. The time percentage that the signal fades below various levels as a function of local time, latitude, season and magnetic index is usually required for a complete evaluation of the expected performance of the proposed systems. The physicist interested in determining the mechanism of scatter or diffraction can utilize the amplitude probability distribution to determine various regimes in which different scattering mechanisms hold. In particular, the distributions will fall into ranges from the strong scattering in the Nakagima q-distribution (approximate Hoyt distribution) through the Rayleigh distribution to the n-weakly scattered distribution (approximate Rice distribution) (Nakagami, 1960; and Bischoff and Chytil, 1969). The model to be shown was developed by converting statistics on scintillation indices to a cumulative amplitude probability distribution function (cdf). The cdf expresses the probability or percentage of time that the signal amplitude will equal or exceed a given amplitude.

3.3 SCINTILLATION INDEX GROUPS AND THEIR CDF MODELS

The scaled values of scintillation index were placed into six groups. Within each group, a range of scintillation indices were encompassed. The groups and ranges of S.I. with their corresponding changes in signal level are shown in Table 3.1.

Table 3.1. Relation of Group to Scintillation Index and Fading

Groups	Scintillation Index (%)	$P_{max}-P_{min}$ (dB)
0	< 20	< 1.7
1	20 - 39	1.7 - 3.6
2	40 - 59	3.7 - 5.9
3	60 - 79	6.0 - 9.4
4	80 - 89	9.5 - 12.7
5	≥ 90	≥ 12.6

Figure 3.1 shows an example of data and the corresponding distribution for each S.I. group. The data for the models were taken utilizing the 150-ft parabola of the Sagamore Hill Radio Observatory. With this antenna, the signals from ATS-3 were recorded at a signal-to-noise ratio of over 30 dB thus insuring sufficient range to record deep negative fades. The output of the receiving system was recorded on magnetic tape. The tape was digitized and the distributions were made by the use of a PDP-9 computer acting as a data processor. Each of the amplitude probability distributions thus obtained for a 15-min segment was then sorted according to the measurement of the simplified scintillation index Eq. (3.1). In order to make each model, many 15-min samples were analyzed in this way. Table 3.2 lists the number of records processed to yield a corresponding median cdf or model distribution.

Table 3.2. Tabulation of Distribution by Groups

S.I. Group	No. of 15-min Distributions
1	49
2	45
3	70
4	50
5	110

A total of 324 distributions was obtained with the division between the S. I. groups as listed. From the sample size for each S. I. group, the median distribution was taken as the central value and called a model distribution for that group. Five model distributions are shown in Figure 3.2. The sixth, group 0, was not measured and is assumed in the model to be constant at the median (0 dB) level. Since group 0 does include small scintillations, less than 20 percent, it is realized that there will be some departure from the median (0 dB) for extreme probabilities. It was estimated, however, that this assumption was justified for engineering applications. The dotted lines, which bracket the group 5 model distribution, define ± three times the standard error of the mean, $\sigma_M = \frac{\sigma}{\sqrt{N}}$, where σ is the standard deviation and N is the number of distributions in the group. This confidence interval is a measure of the probable extent to which a model distribution of group 5 is apt to vary with future samplings. The limits defined by $\pm 3\sigma_M$ for the model distributions of the other S. I. groups were comparable to those shown for group 5. The number of samples in group 5 was deliberately made larger than the others to increase accuracy for extreme deviations from the median level.

As will be shown later, the individual 15-min distributions closely followed the Nagakami m-distribution and could therefore be related to a particular value of the m-parameter. Since the individual distributions which comprise each S. I. group agree closely with Nakagami distributions, the median for each group is also a Nakagami distribution. In Figure 3.2 the curves are solid over the range that the median, of the experimentally determined distributions, agreed with a theoretical m-distribution within 0.5 dB. Experimental accuracy was not sufficient to determine the extreme values, and the dotted lines are extended in accordance with the theoretical m-distributions for values of m given in the parenthesis.

The model distributions shown in Figure 3.2 are used in the following manner to determine a cdf which corresponds to the frequency of occurrence of the S. I. groups for a given period. The percent occurrence of each S. I. group is multiplied by its probability at each dB level, as given in Figure 3.2, and the values summed to give a composite curve. Expressed mathematically:

$$\mathrm{cdf(dB)} = \sum_{\mathrm{Group}=0}^{5} f(G)\, P(dB)$$

where $f(G)$ is the frequency of occurrence of a group and $P(dB)$ is the probability or percent of time at each dB level from Figure 3.2. Three distributions are shown in Figure 3.3 representing the conversion of occurrence statistics for two years of data for Hamilton, Mass. Daytime and nighttime variations are separated from all hours. It is noted that a weighted combination of Nakagami distributions produces a composite curve which cannot be represented by a Nakagami distribution.

A question naturally arises concerning the validity of determining a cumulative-amplitude-probability-distribution function in the described manner. One method of determining the validity and accuracy of the conversion process is to compare a derived distribution with one that is well known. During the period 25-30 July 1970, several periods of large scintillations were recorded on the 136 MHz signal from ATS-3. The use of the 150-ft antenna for receiving the signal allowed adequate signal-to-noise ratio for measuring the deepest fades. Since the ATS-3 signal is essentially linearly polarized, a circularly polarized feed was used to eliminate the undesirable effects of Faraday rotation. A total of 35.5 hr of scintillations was recorded, digitized, and processed on a computer to determine the cumulative amplitude distribution shown as the solid curve in Figure 3.4. For the same scintillation period, 15-min scintillation indices were scaled and the percent occurrence of the S. I. groups were converted to a cdf using the model distributions of Figure 3.2. The percent occurrence values were multiplied by the percent of time for each S. I. model distribution and the values summed to give the dashed curve on Figure 3.4. The comparison in Figure 3.4 of the derived distribution with the actual distribution, shows that the distributions agree within 0.5 dB for the abscissa range of 0.1 to greater than 99.9. It is felt that this test demonstrates that distributions can be obtained from the modelling process with sufficient accuracy for engineering applications for midlatitude stations.

3.4 HIGH LATITUDE CDF

Measurements in the auroral region and at the equator show a considerable increase in the occurrence of deep scintillation over that experienced at midlatitudes. A large data base of S. I. measurements was available from stations in Greenland and Peru. It was proposed that the distribution models (Figure 3.2) determined from Hamilton, Mass. data could also be applied to convert S. I. measurements from other sites to a cdf and thus determine fading margins for other geographical regions. To determine the validity of the conversion technique for other latitudes, the following procedure was used. From the signal-strength records for each of the other sites, cumulative distributions were manually scaled. The solid curve in Figure 3.5 is the distribution for Narssarssuaq, Greenland which was obtained by scaling 10.25 hr of strip charts which displayed a range of scintillations. The solid curve in Figure 3.6 is the distribution for Huancayo, Peru and represents 7 hr of scintillating data. For each of the sets of data, the occurrence of the 15-min S. I. was found as tabulated by groups on Figures 3.5 and 3.6. The occurrence values of the S. I. groups were then converted to a distribution using the models (Figure 3.2) from Hamilton data, and shown as dashed

curves on Figures 3.5 and 3.6. Figu. e 3.5 for the auroral region shows that the modelling process gives a distribution that compares with the manually obtained distribution within 1 dB for the percentile range of 1 to greater than 99. Comparison of the two distributions in Figure 3.6 for the equatorial region shows a significant departure for percentiles less than 1 and greater than 98. This could be a real effect in that a group 5 model for Peru could give greater changes in amplitude in the extreme percentile ranges; that is, it would be represented by a smaller value of m than was found for Hamilton data, or it could be that the sample size of 7-hr was not large enough for statistical comparison. It is concluded, however, that the tests which have been described have shown that the models of Figure 3 2 can be used to convert archive data in the form of scintillation indices to cdf's for midlatitude and auroral regions with sufficient accuracy for engineering applications and over a more limited percentile range for the equatorial region.

3.5. ENGINEERING USES OF SCINTILLATION INDICES

It should be noted that there are two distinct ways in which the occurrence of the S.I. groups can be utilized.

(1) A cdf can be determined in the previously described manner. This would allow a fading margin to be determined to overcome this propagation effect for whatever conditions are represented by the statistical sort of the S.I. values.

(2) Relate the depth and occurrence of fading to the particular modulation techniques. For certain modulation systems (very high-speed pulse code for example), if the signal fell below threshold for acceptable signal) only a small percentage of a 15-min period, then the entire 15-min period might be useless unless some form of redundancy were used. Therefore, it is important to list the percentage of time each of the scintillation ranges (and therefore model distributions) occurred for each set of magnetic indices. Projected occurrence of magnetic indices will allow the engineer to forecast occurrence of system disruption. In Table 3.3 we have listed magnetic index variations.

Table 3.3. Percentage of Occurrence of Magnetic Index Sets

Year	K_p = 0-3	K_p = 4-9
1950	72.8	27.2
1951	63.5	36.5
1952	64.2	35.8
1953	75.3	24.7

Table 3.3 (Contd.). Percentage of Occurrence of Magnetic Index Sets

Year	$K_p = 0-3$	$K_p = 4-9$
1954	85.6	13.4
1955	85.9	14.1
1956	74.7	25.3
1957	72.9	27.1
1958	71.6	28.4
1959	68.5	21.5
1960	67.3	32.7
1961	81.7	18.3
1962	82.2	17.8
1963	82.7	17.3
1964	88.0	12.0
1965	93.3	6.7
1966	88.4	11.6
1967	86.6	13.4
1968	81.9	18.1
1969	87.4	12.6
1970	86.8	13.2
1971	85.4	14.6

3.6 THE NAKAGAMI DISTRIBUTION

The method described in this report was developed as a means of converting archive data of scintillation indices to a cdf. The tests on the accuracy of the method indicate that it is sufficient for engineering applications, except possibly in the extreme percentiles and for the equatorial region. An analysis of a greater number of 15-min distributions of the group 5 category is necessary for equatorial scintillations to determine if the model of Figure 3.2 will fit that area.

Bischoff and Chytil (1969) showed that an approximate measure of scintillation index, Eq. (3.1) and the exact measures of Briggs and Parkin (1963) were closely related. In their analysis, Bischoff and Chytil have used Nakagami's m distribution as a measure of scintillations. The distribution function of intensity X (dB) is given by:

$$p(X) = \frac{2 \, m^m}{M \, \Gamma(m)} \, \exp\left[m \left(\frac{2X}{M} - e^{2X/M} \right) \right] \tag{3.2}$$

where $M = 20 \log_{10} e = 8.686$. A plot of the cumulative distribution is shown on Figure 3.7, for several values of m from 1 to 40. Even though only integer values are shown, m is continuously variable and can have any value ≥ 0.5. It is also evident that the fading range is proportional to $1/m$.

Six experimental 15-min distributions from group 5 and four distributions from group 4 are plotted in Figure 3.8. The two solid curves are the theoretical distributions with $m = 1$ and 1.3 and the dashed curve is $m = 4$. No test of fitness was made, but, since m can have other closely spaced values to those shown, visual inspection leads to the conclusion that there is good agreement between the theoretical curves and the experimental distributions.

Experimentally obtained distributions from S. I. groups 3, 2, and 1 have been found to agree with theoretical distributions having m values ranging from 6 through 100. Since the 15-min distributions agree very closely with the theoretical m distributions over the measurement range, extreme values can be approximated from the theoretical curves when required. For example, a fade depth of -27 dB is indicated for the 99.9 percentile for the $m = 1$ distribution.

3.7 FREQUENCY DEPENDENCE

The frequency of a system in the design study phase can be a variable with the choice at times within only a short range (225 MHz to 400 MHz, for example) or between frequencies differing by an order of magnitude (136 MHz to 1550 MHz). With available data the tradeoffs possible can be evaluated at middle and high latitudes in the first case with a fair degree of certainty.

The frequency dependence can be determined by relating the ratio of the amount of power in the scintillating component to the frequency ratio. Aarons et al. (1967) determined the frequency dependence of radio star scintillations from the relationship:

$$\eta = \log \frac{S_1}{S_2} / \log \frac{f_1}{f_2} \qquad (3.3)$$

where S is the scintillation index of Eq. (3.1). η is termed the spectral index of the scintillations. This expression is valid as long as S is a constant power law function of frequency. A log-log plot of S vs f will result in a straight line with a slope equal to η. Their results show that the scintillation index is inversely proportional to frequency squared for weak scintillations, and approaches a $1/f$ dependence for high levels of scintillation. As pointed out earlier, however, scintillation index is not a convenient system design or physical parameter.

It has been shown (Chytil, 1967) that:

$$S_4 = \sqrt{1/m} \text{ for } m \geq 0.5 \tag{3.4}$$

where S_4 is the notation used by Briggs and Parkin (1963) to measure the scintilla-tion depth as the root-mean-square power deviation divided by the mean power, and m is Nakagami's parameter.

By substituting $\sqrt{1/m}$ for S in Eq. (3.3), it can be found that:

$$-\angle \eta = \log \frac{m_1}{m_2} \Big/ \log \frac{f_1}{f_2} = \eta_m \ . \tag{3.5}$$

If η_m can be evaluated from simultaneous distributions for two frequencies from the same source, then prediction of the expected distribution at a desired fre-quency can be made as long as scintillation index and m remain a constant power of frequency.

The technique is illustrated in Figure 3.9 which shows the experimentally determined cdf's for two frequencies. By comparing the experimental distribu-tions with the theoretical distributions, it can be seen that these distributions approximately follow a theoretical distribution of $m = 1.5$ for 137 MHz and $m = 40$ for 412 MHz. Evaluation of η_m gives:

$$\eta_m = \log \frac{1.5}{40} \Big/ \log \frac{137}{412} = 2.98 \ . \tag{3.6}$$

[From Eq. (3.5) this value of η_m would correspond to a scintillation index spectral law of -1.5]. Using the value of η_m from Eq. (3.6) and assuming that a constant power law relationship holds over the frequency interval, a predicted distribution with $m = 9.5$ would be obtained at 254 MHz.

If strong scattering is observed, that is, $0.5 \leq m \leq 1$ on the lower frequency, a constant power law relationship may not be the case and interpolation or extrapolation for a distribution at other frequencies may be untenable.

To determine the spread in experimentally determined values of spectral index η_m, 22 simultaneous records of scintillations at 137 and 412 MHz were processed to give corresponding 15-min cumulative amplitude distributions. The values of m varied from 1.1 to 4.9 at the lower frequency and from 24 to 100 at the higher frequency. Spectral indices were calculated from the values of m and frequency of occurrence is shown in Figure 3.10. The data peaks in the range of 2.8 to 3.1.

3.8 ANGLE OF ELEVATION EFFECTS

The basic formula for describing the effect of angle of elevation on scintillation is given by Briggs and Parkin (1963):

$$S \propto \lambda \ (\sec i)^{1/2} \left\{ 1 + \frac{\Pi^2 L_c^4}{4\lambda^2 Z^2} \right\}^{-1/2}$$

The difficulty in testing the equation is that in practical situations, the propagation path to two synchronous satellites traverses two differing invariant latitudes. For a short period (15 January to 15 April 1968) simultaneous data from ATS-3 and Canary Bird were compared utilizing the cdf technique. Figure 3.11(a) graphs the results of a comparison for one satellite, Canary Bird, at approximately 11° of elevation with that of ATS-3 at 37° of elevation. The graph in Figure 3.11(b) is obtained by plotting the corresponding dB levels for the same percentage of time from Figure 3.11(a) for the two satellites. The slope of the latter curve is 1.28.

The intersection latitude of the two paths differed somewhat. This, coupled with the necessity of placing measurements into their proper context as to falling within near or far field considerations (Aarons et al, 1971), does not allow us to generalize further on angle of elevation effects. The observations approximate theoretical values but are too meager to be definitive.

3.9 SUNSPOT NUMBER AND MAGNETIC INDEX OCCURRENCE

A parameter of obvious importance in geophysics is the solar flux or sunspot number. It has been shown that years of high sunspot number show an increase in mean scintillation index relative to years of low sunspot number (Lansinger and Fremouw, 1967). A comparison of measurements for the effect of sunspot number must, however, normalize for the occurrence of magnetic index values. Years of high sunspot number bring a high occurrence of magnetic storms. Greater scintillation activity may be the result of more magnetic storms. Aarons et al (1964) have shown that during magnetically quiet periods (K = 0, 1, 2), increasing sunspot number increases scintillation index but it is of lesser importance than magnetic index.

The data base on which the present statistical study rests is not long enough in time to allow a sunspot number parameter to emerge as a variable. A separation of the cdf's as a function of K groupings, however, has been made. The projected occurrence of K indices can then be utilized to evaluate scintillations for a particular year. In Table 3.3, we gave the occurrence of Kp from 1950 to 1971. In Figure 3.12

we have graphed the occurrence of Kp = 0, 1 and Kp 4-9. It is clear from the table and the graph that the occurrence pattern of quiet and disturbed magnetic indices differ significantly from the sunspot number of 10-cm solar flux parameters.

The data base used for the observations listed in Appendix A are predominantly from 1968, 1969, and 1970.

3.16 DIURNAL AND SEASONAL DEPENDENCE

The descriptive model of the irregularity region indicates it is possible to characterize a geomagnetic latitude by the occurrence of scintillation index groups. The occurrence of scintillations at one location is a function of:

(1) Local propagation path intersection time (more properly corrected geo-magnetic time).

(2) Season.

(3) Planetary or local magnetic index.

In this statistical model of fading occurrence, we treat only three latitudes. The first is that of the propagation path from Sagamore Hill through an invariant latitude of 54° (at 350 km altitude). The second is that of a path through a latitude of 64° (Narssarssuaq) and the third through 77° (Thule). The typical angle of elevation to ATS-3, the source used for this data, was 40° for Sagamore Hill, 13° for Narssarssuaq, and 4° for Thule. The synchronous satellite was near its maximum elevation angle for this study (the satellite was positioned near station longitude for two of the observatories for a large portion of the period of data taking). The data has not been normalized for angle of elevation effects; without normalization it is felt that the data represents a practical situation for the three latitudes.

In Appendix A, the percentage of occurrence of scintillation indices are listed for hourly groupings of local time, seasons, and magnetic index sets. We have also transformed these into cumulative amplitude probability tables.

It is hoped that the tables will be of use in evaluating the effect of scintillations on proposed systems involving high latitude propagation paths from satellites.

References

Aarons, J., Mullen, J.P. and Basu, S. (1964) The statistics of satellite scintillation at a subauroral latitude, J. Geophys. Res. 69:1785-1794.

Aarons, J., Allen, R.S. and Elkins, T.J. (1967) Frequency dependence of radio star scintillations, J. Geophys. Res. 72:2891-2902.

Aarons, J., Whitney, H.E. and Allen, R.S. (1971) Global morphology of ionospheric scintillation, Proc. IEEE 59(No. 2):159-172.

Bischoff, K. and Chytil, B. (1969) A note on scintillation indices, Planet. Space Sci. 17:*566-1069.

Briggs, B.H. and Parkin, I.A. (1963) On the variation of radio star and satellite scintillations with zenith angle, J. Atmos. Terr. Phys. 25:339.

Chytil, B. (1967) The distribution of amplitude scintillation and the conversion of scintillation indices, J. Atmos. Terr. Phys. 29:1175-1177.

Lansinger, J.M. and Fremouw, E.J. (1967) The scale size of scintillation-producing irregularities in the auroral ionosphere, J. Atmos. Terr. Phys. 29:1229-1242.

Nakagami, M. (1960) Statistical methods in Radio Wave Propagation, Pergamon Press, pp 3-36.

Whitney, H.E., Malik, C. and Aarons, J. (1969) A proposed index for measuring ionospheric scintillation, Planet. Space Sci. 17:1069-1073.
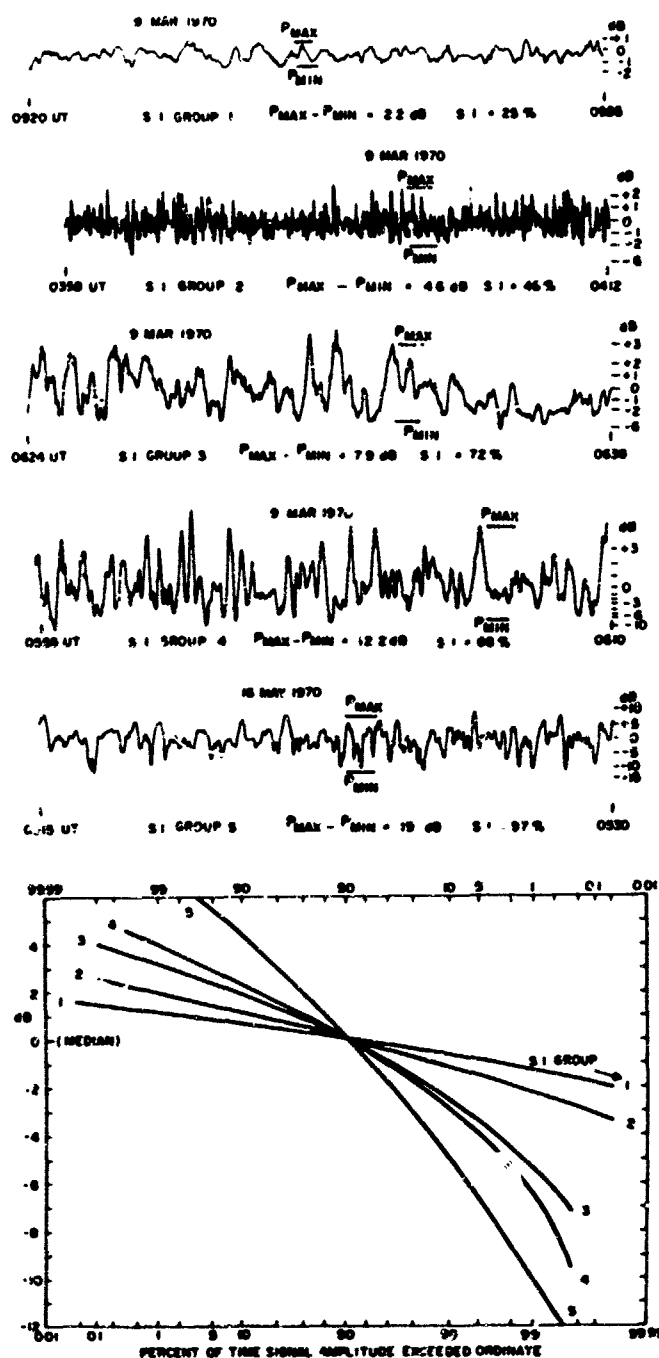
Figure 3.1. Examples of Scintillation Data for Each of the Five S. I. Groups and the Resulting Cumulative Amplitude Probability Distribution Functions (cdf). Records were obtained from ATS-3 transmissions at 136 MHz
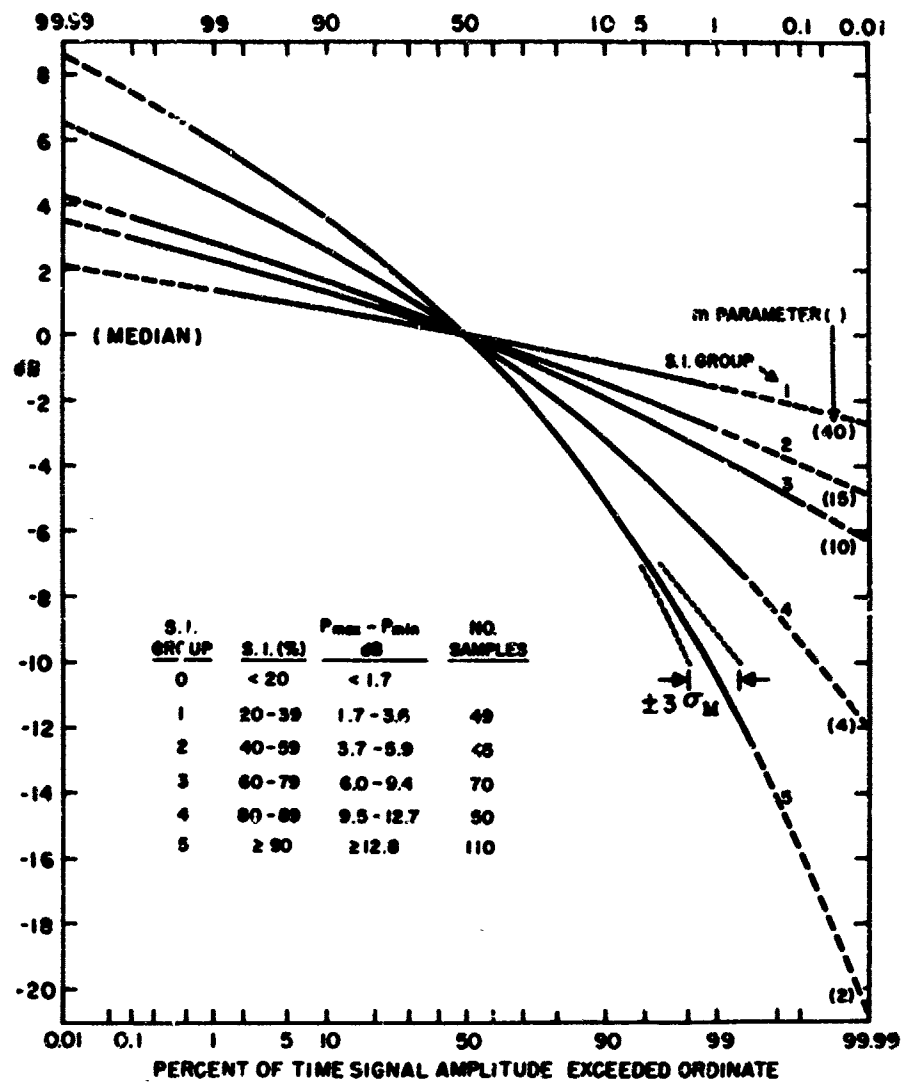
Figure 3.2. Median (Model) Distributions Obtained From the Sample Size for Each S. I. Group From ATS-3 Data Recorded at Hamilton, Mass. Solid curves denote the range of the experimental data; dashed curves denote an extension based on the Nakagami distribution for the value of m in parentheses. σ_M equals standard error of the mean
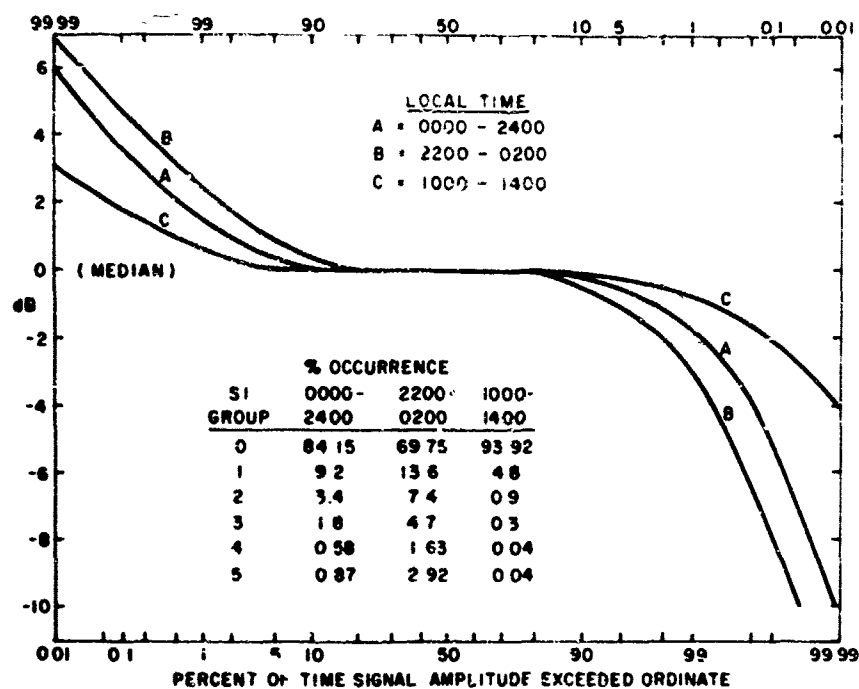
Figure 3.3. Cumulative Distributions for Approximately Two Years of ATS-3 Data at 136 MHz From Hamilton, Mass. These were obtained by the conversion of occurrence statistics of scintillation indices (K 0-9) and the use of the distributions in Figure 3.2. The day-to-night variation is shown

44
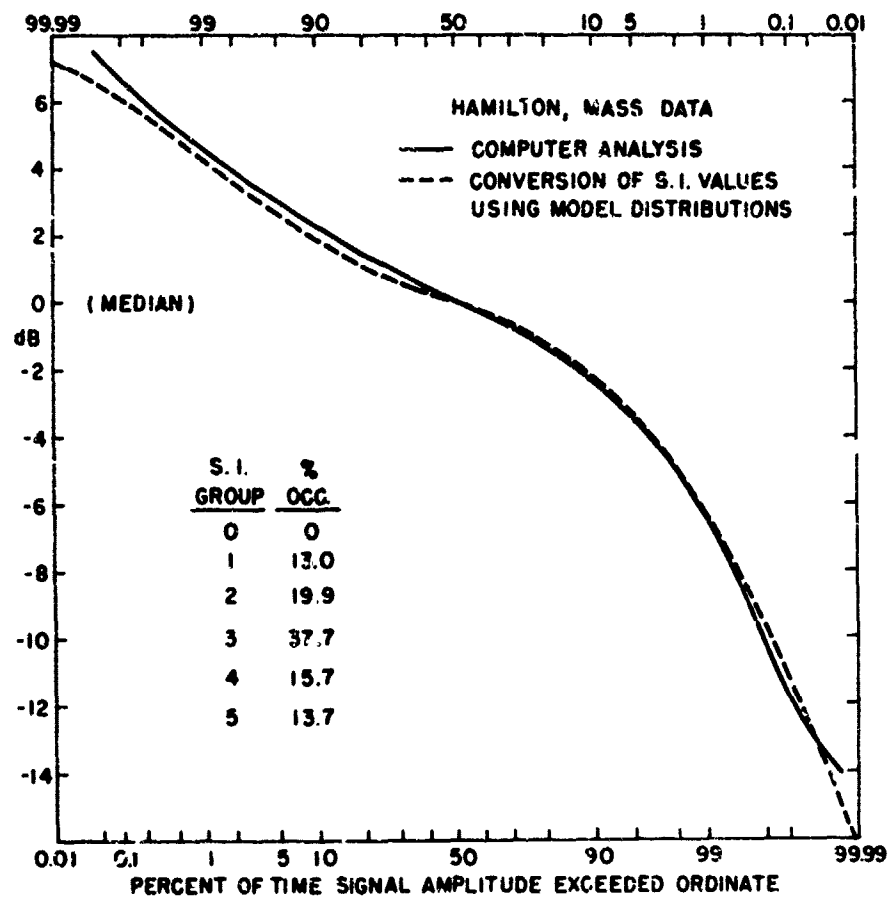
Figure 3.4. Comparison of an Actual Dis*ribution for 35.5 hr of Data (136 MHz) Obtained by Computer Analysis Witn the Distribu*ion Obtained by the Conversion of the Occurrence of S. I. Groups for the Same Period
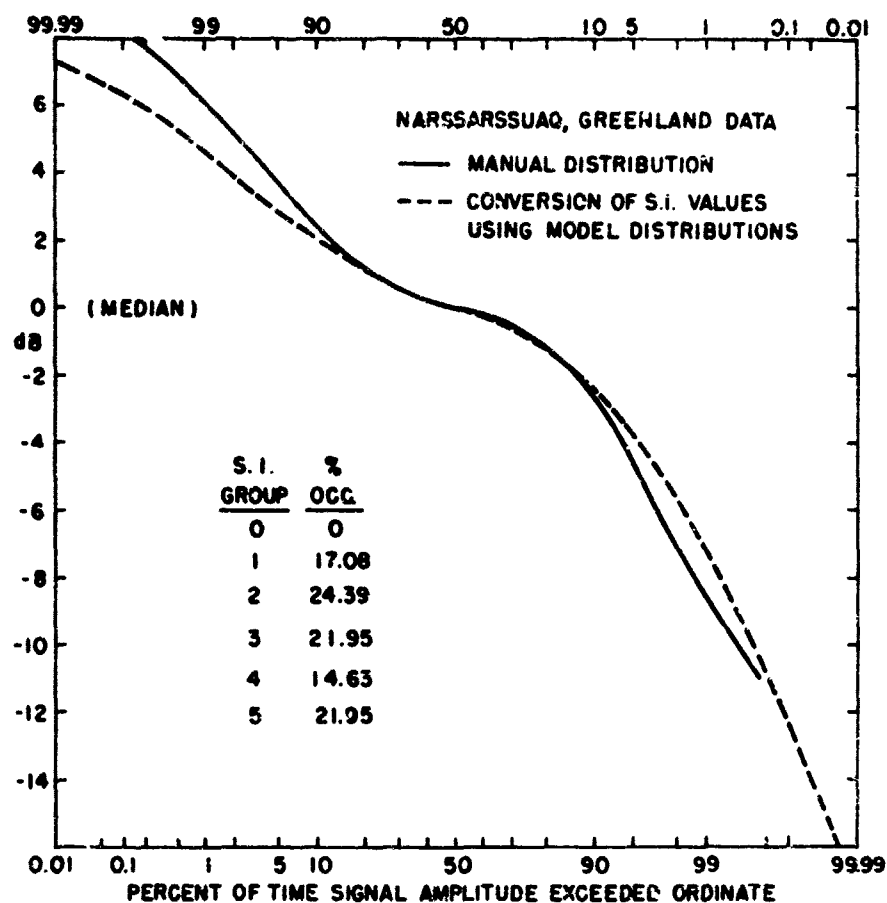
Figure 3.5. Comparison of an Actual Distribution for 10.25 hr of Data
(136 MHz) Taken at Narssarssuaq, Greenland, With the Distribution
Obtained From the Hamilton, Mass. Models for the Same Period
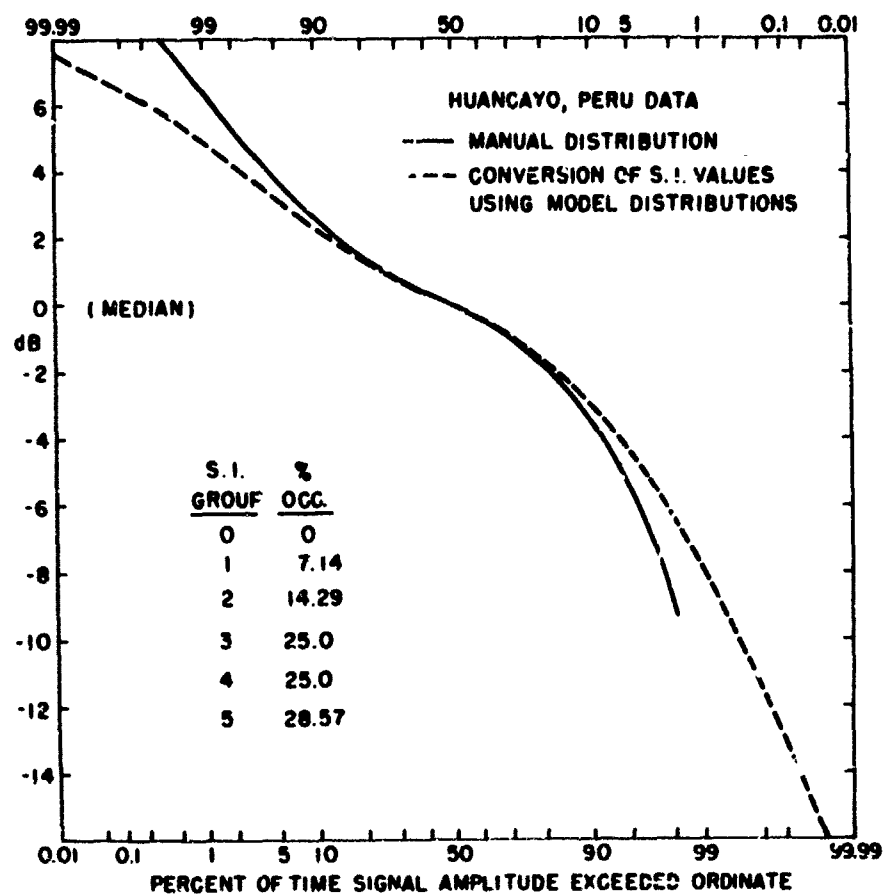
Figure 3.6. Comparison of an Actual Distribution for 7 hr of Data (136 MHz) Taker. at Huancayo, Peru, With the Distribution Obtained From the Hamilton, Mass. Models for the Same Period
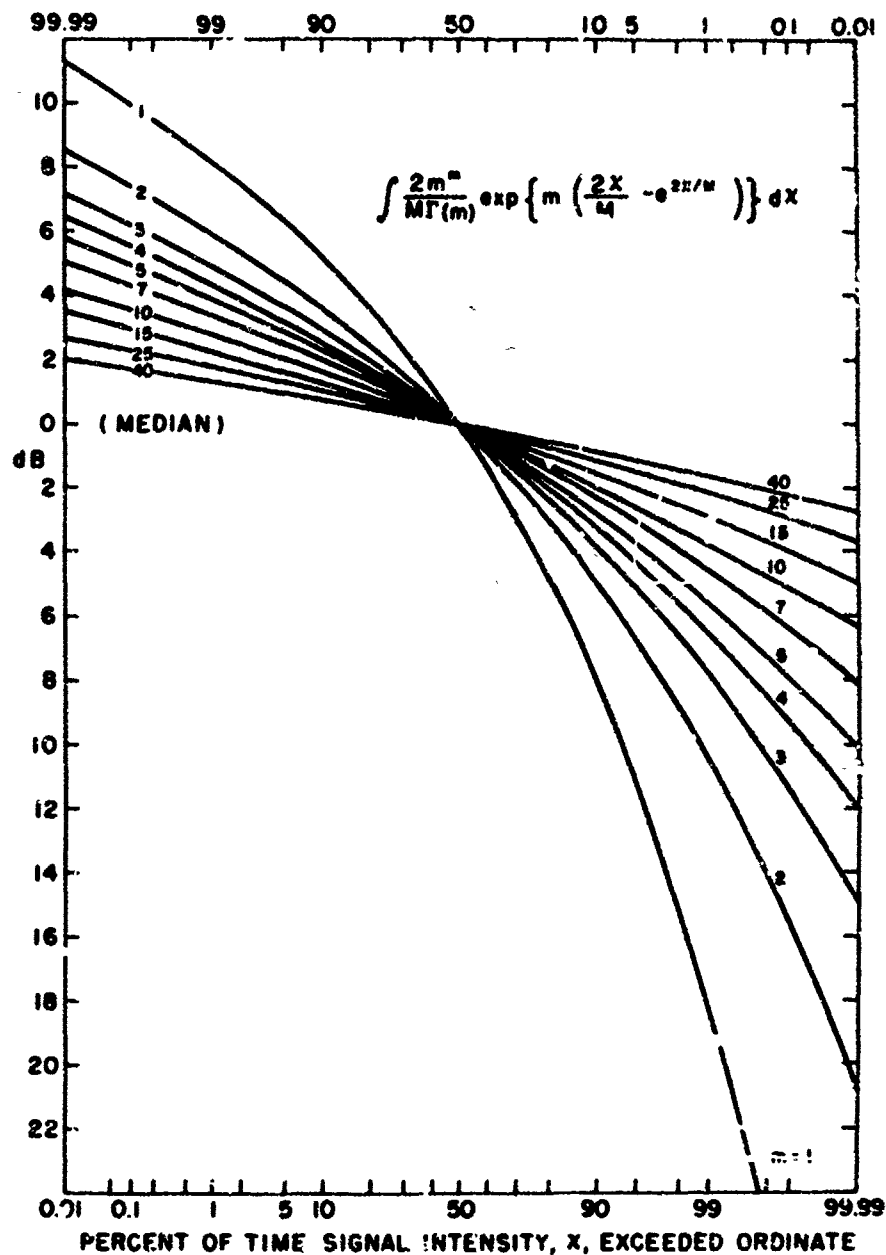
Figure 3.7. Cumulative Form of the Nakagami Distribution: Valid for $m \geq 0.5$
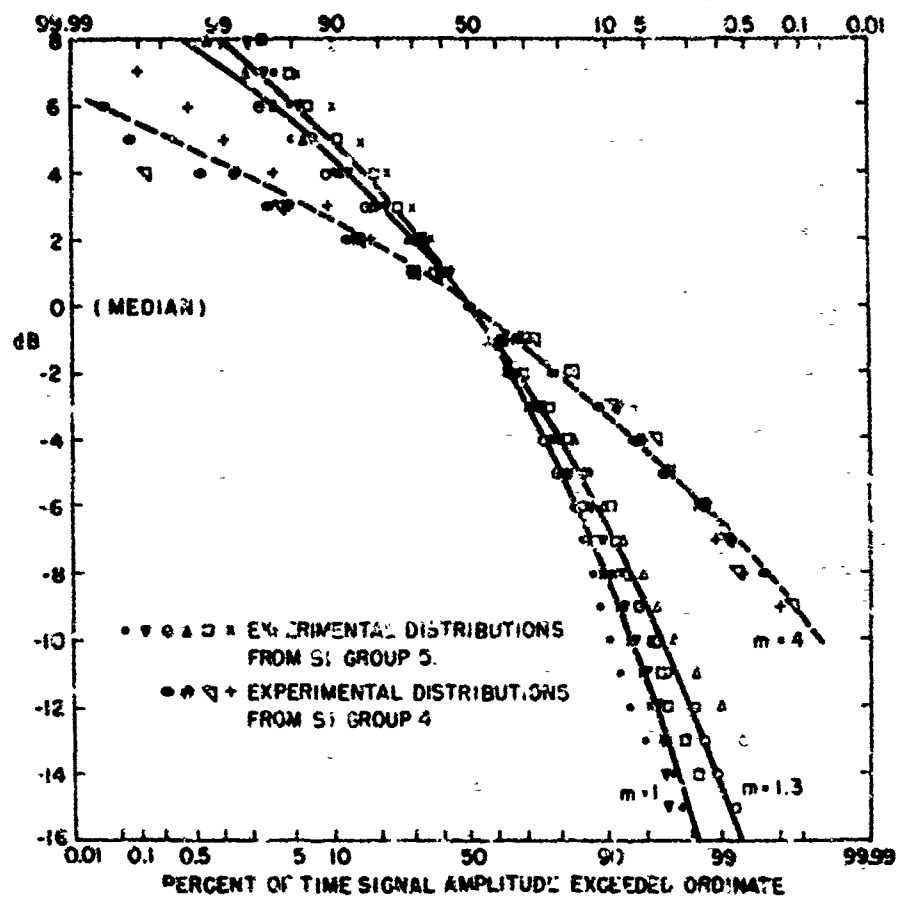
Figure 3.8. Comparison of Theoretical m-Distributions (Solid Line for $m = 1$ and 1.? Dashed for $m = 4$) With Experimental Distributions Fro i. L. Groups 4 and 5
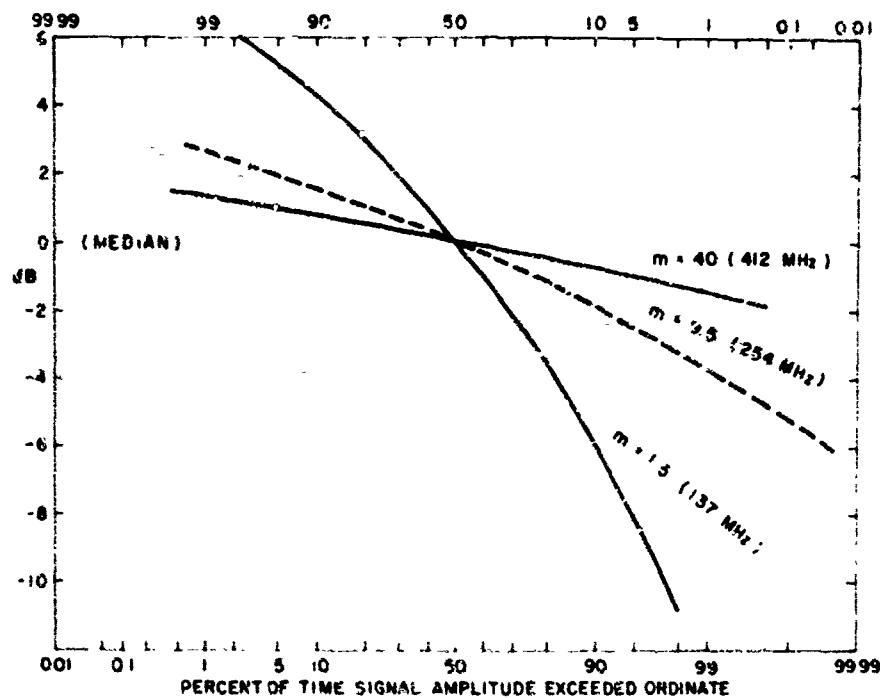
Figure 3.9. The Solid Lines Are the Experimentally Measured Distributions for Simultaneous Recordings of ATS-3 data. The dashed line is an estimated distribution for 254 MHz which was arrived at by interpolating the measurements with the spectral index, n_m, as follows:

$$\eta_m = \log \frac{m_1}{m_2} / \log \frac{f_1}{f_2} = 2.98$$
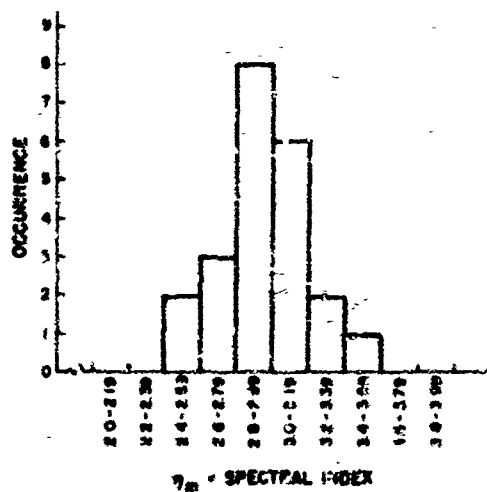
Figure 3-10. Occurrence of Spectral Index Values From a Data Base of 22 Pairs of 15 Min Amplitude Distributions of 137 and 412 MHz Signals where:

$$\eta_m = \log \frac{m_1}{m_2} / \log \frac{f_1}{f_2}$$

m = Nakagami's Distribution Parameter, and

f = Frequency
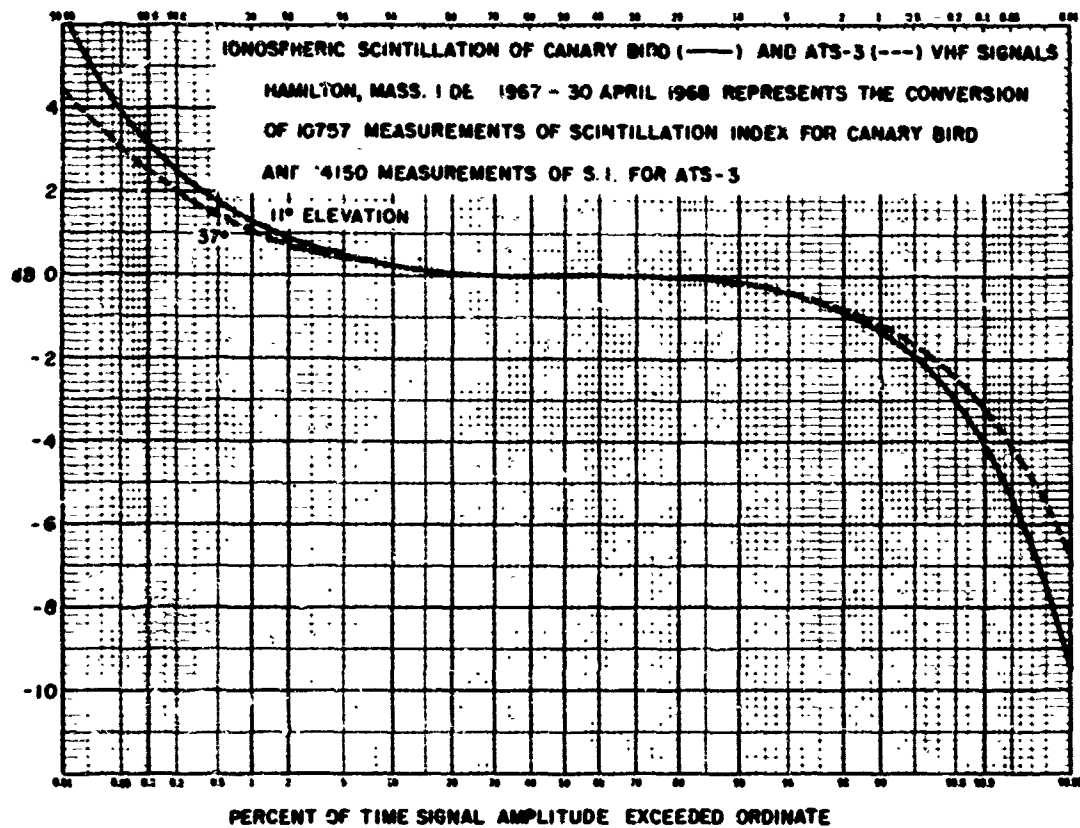
Figure 3 11a. Percent of Time Signal Amplitude Exceeded Ordinate
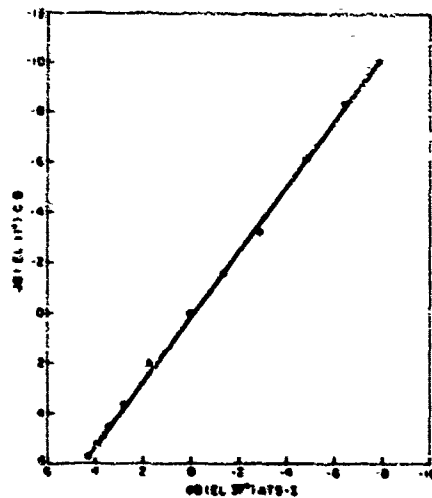
Figure 3-11b. Comparison of
Amplitude Probabilities for the
Two Paths. Slope is 1.28
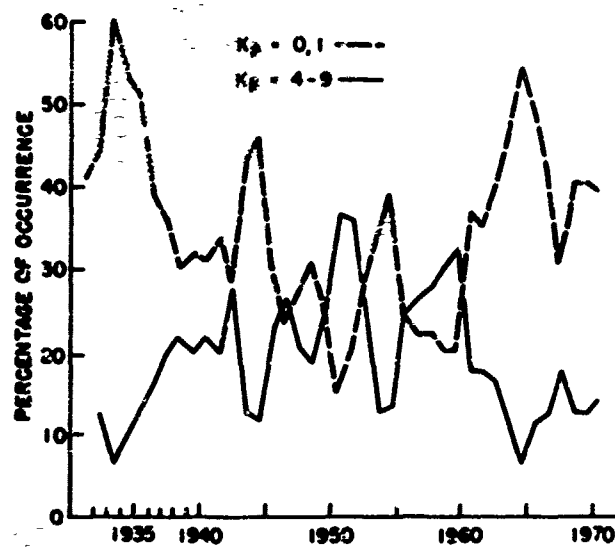
Figure 3. .... Variation of Occurrence of Very Quiet
Magnetic Indices (K_p = 0, 1) and Disturbed Indices
(K_p = 4-9) through 1971

Appendix A

Cumulative Amplitude Probability Distributions

The following data pages contain analyzed cdf's for the three sites used in the test. Seasonal patterns are shown as well as cdf's for all the data available. Thule seasonal patterns are not given since the data base was judged inadequate.

In the cdf's, the symbol A is placed alongside values where the accuracy of the interpolation routine is doubtful; the symbol B is placed alongside values where the data is extrapolated and also may be doubtful.

HAMILTON ATS-3　　　　　NOV-JAN　　　1969-72　　　LOCAL TIME
X=0-3

DIURNAL VARIATION

SI	00-24 PCT	10-14 PCT	14-18 PCT	18-22 PCT	22-02 PCT	02-06 PCT	06-10 PCT
00-19	82.92	95.30	90.95	86.93	62.52	71.42	90.18
20-39	11.08	3.46	8.32	9.38	18.76	18.50	8.02
40-59	3.78	1.36	.60	2.22	11.10	6.25	1.68
60-79	1.42	.18	.09	.93	4.68	2.55	.17
80-89	.28	0.00	.04	.27	.58	.43	0.00
90-99	.51	0.00	0.00	.27	1.56	.85	.04

DIURNAL VARIATION

PCT	00-24 DB	X	10-14 DB	X	14-18 DB	X	18-22 DB	X	22-02 DB	X	02-06 DB	X	06-10 DB	X
.05	4.51		2.15		2.22		3.96		6.54		5.21		2.53	
.10	3.65		1.76		1.84		3.07		5.42		4.29		2.08	
.20	2.83		1.39		1.51		2.37		4.41		3.43		1.68	
.50	1.94		.35		1.12		1.61		3.22		2.42		1.23	
1.00	1.41		.56		.87		1.17		2.41		1.80		.94	
2.00	.99		.42		.66		.84		1.72		1.29		.68	
5.00	.57		.17		.41		.48		1.02		.77		.41	
10.00	.34		.35		.26		.29		.61		.49		.25	
20.00	.16		-.01		.12		.15		.25		.25		.12	
30.00	.08		.01		.06		.08		.13		.10		.05	
40.00	.01		.00		.02		.01		.05		.04		.02	
50.00	0.00		0.00		0.00		0.00		0.00		0.00		0.00	
60.00	.00		.32		-.00		.01		-.04		-.03		-.00	
70.00	.01		.13		.05		.03		-.18		-.06		.05	
80.00	-.04		.31	A	.05		.00		-.24		-.16		.04	
90.00	-.22		.30	A	-.04	A	-.13		-.61		-.43		-.06	A
95.00	-.52		.14	A	-.23		-.38		-1.12		-.82		-.26	
98.00	-1.09		-.36		-.59		-.87		-2.08		-1.50		-.65	
59.00	-1.65		-.61		-.92		-1.35		-2.79		-2.12		-1.83	
99.59	-2.27		-1.35		-1.33		-1.92		-3.82		-2.62		-1.46	
99.80	-3.35		-1.55		-1.88		-2.78		-5.56		-4.89		-2.06	
99.90	-4.35		-2.12		-2.30		-3.67		-7.48		-5.28		-2.51	
99.95	-5.73		-2.59		-2.78		-4.65		-9.27		-7.04		-3.84	

HAMILTON ATS-3　　　　　FEB-APR　　　1969-72　　　LOCAL TIME
X=0-3

DIURNAL VARIATION

SI	00-24 PCT	10-14 PCT	14-18 PCT	18-22 PCT	22-02 PCT	02-06 PCT	06-10 PCT
00-19	84.63	96.98	97.29	84.78	64.34	78.86	94.86
20-39	7.49	2.58	2.56	9.22	12.52	12.68	5.83
40-59	3.32	.15	.10	2.59	8.35	7.58	.66
60-79	2.34	0.00	.05	1.71	6.58	5.36	.19
80-89	.87	.19	0.00	.93	2.41	1.64	.05
90-99	1.35	.00	0.00	.78	5.80	1.35	0.00

DIURNAL VARIATION

PCT	00-24 DB	X	10-14 DB	X	14-18 DB	X	18-22 DB	X	22-02 DB	X	02-06 DB	X	06-10 DB	X
.05	5.94		1.98		1.56		5.23		7.85		6.34		2.19	
.10	4.86		1.30		1.26		4.28		7.07		5.23		1.78	
.20	3.91		1.12		1.01		3.35		5.96		4.32		1.42	
.50	2.62		.96		.71		2.22		4.54		3.15		1.01	
1.00	1.79		.57	A	.53		1.54		3.52		2.36		.74	
2.00	1.13		.42	A	.38		1.00		2.46		1.66		.52	
5.00	.50		.29	A	.21		.49		1.29		.51		.29	
10.00	.19		.20	A	.12		.24		.63		.48		.16	
20.00	.02		.13	A	.05		.08		.28		.19		.07	
30.00	-.01		.07	A	.01		.03		.05		.07		.02	
40.00	-.02		-.02		.00		-.01		.02		.03		.01	
50.00	0.00		0.00		0.00		0.00		0.00		0.00		0.00	
60.00	.05		.04		.02		.03		.01		-.01		.01	
70.00	.08		.08		.14		.04		-.02		-.02		.39	
80.00	.06		.12		.20	A	.02		-.17		-.13		.12	A
90.00	-.12		.12		.22	A	-.14		-.66		-.47		.87	A
95.00	-.48		.15		.14	A	-.45		-1.42		-.98		-.07	A
98.00	-1.25		-.16		-.09	A	-1.11		-2.79		-1.98		-.48	
99.00	-2.85		-.42		-.34	A	-1.07		-4.19		-2.72		-.71	
99.50	-3.82		-.75		-.61		-2.58		-5.84		-3.75		-1.13	
99.80	-4.75		-1.31		-1.14		-4.84		-8.40		-5.37		-1.72	
99.90	-6.41		-1.84		-1.54		-5.30		-10.48		-7.04		-2.18	
99.95	-8.31		-2.48		-1.95		-7.67		-12.65		-8.82		-2.64	

HAMILTON ATS-3   MAY-JUL   1969-72   LCCAL TIME
K=0-3

DIURNAL VARIATION

SI	00-24 PCT	10-14 PCT	14-18 PCT	18-22 PCT	22-02 PCT	02-06 PCT	06-10 PCT
00-19	90.74	94.94	96.81	88.26	81.58	87.88	95.24
20-39	5.34	4.29	2.90	6.30	7.47	7.09	3.84
40-59	2.01	.61	.27	2.75	4.80	2.86	.69
60-79	1.01	.10	.03	1.36	3.18	1.16	.19
80-89	.33	.03	0.00	.47	.96	.56	.03
90-99	.57	.33	0.00	.85	2.10	.44	0.00

CIURNAL VARIATION

PCT	00-24 DB	X	10-14 DB	X	14-18 DB	X	18-22 DB	X	22-02 DB	X	02-06 DB	X	06-10 DB	X
.05	4.61		2.14		1.67		5.18		6.58		4.46		2.12	
.10	3.67		1.70		1.36		4.20		5.46		3.61		1.71	
.20	2.73		1.33		1.08		3.21		4.45		2.78		1.35	
.50	1.71		.35		.76		2.06		3.09		1.85		.93	
1.00	1.14		.71		.55		1.30		2.15		1.29		.67	
2.00	.71		.52		.38		.87		1.38		.85		.44	
5.00	.33		.32		.19		.40		.60		.42		.22	
10.00	.15	A	.21		.10		.17		.25		.20		.16	
20.00	.05	A	.11		.03		.05		.03		.07		.03	
30.00	.02		.01		.02		.01		-.02		.02		.01	
40.00	-.03		.00		.00		-.03		-.02		-.01		.00	
50.00	0.00		0.00		0.00		0.00		0.00		0.00		0.00	
60.30	.04		.02		.02		.04		.05		.03		.02	
70.06	.07		.09		.13		.07		.07		.06		.12	
80.88	.09		.12		.19	A	.07		.04		.05		.16	A
90.88	-.00		.08	A	.20	A	-.05		-.19		-.07		.14	A
95.00	-.22		-.04		.11	A	-.33		-.64		-.34		.01	A
98.80	-.73		-.35		-.14	A	-.93		-1.55		-.90		-.31	
99.00	-1.28		-.64		-.42		-1.58		-2.45		-1.47		-.68	
99.50	-1.99		-1.34		-.72		-2.37		-3.63		-2.16		-1.02	
99.88	-3.10		-1.62		-1.26		-3.82		-5.68		-3.29		-1.61	
99.90	-4.40		-2.10		-1.67		-5.21		-7.32		-4.36		-2.08	
99.95	-5.95		-2.57		-2.08		-7.02		-9.44		-5.72		-2.55	

HAMILTON ATS-3   AUG-OCT   1969-72   LCCAL TIME
K=0-3

CIURNAL VARIATION

SI	00-24 PCT	10-14 PCT	14-18 PCT	18-22 PCT	22-02 PCT	02-06 PCT	06-10 PCT
00-19	86.46	91.41	91.35	81.37	78.24	84.67	91.39
20-39	9.08	7.20	7.76	11.91	9.91	10.06	7.67
40-59	2.23	.97	.79	3.48	4.81	2.80	.66
60-79	1.17	.32	.89	1.34	3.48	1.74	.23
80-89	.41	.35	0.00	.97	1.21	.19	.05
90-99	.64	.05	0.00	.93	2.43	.53	0.00

DIURNAL VARIATION

PCT	00-24 DB	X	10-14 DB	X	14-18 CB	X	18-22 CB	X	22-02 CB	X	02-06 DB	X	06-10 DB	X
.05	4.79		2.38		2.18		5.44		6.86		4.53		2.34	
.10	3.86		2.07		1.83		4.42		5.71		3.68		1.91	
.29	2.92		1.64		1.51		3.49		4.65		2.82		1.54	
.50	1.88		1.17		1.12		2.33		3.32		1.98		1.13	
1.00	1.30		.96		.86		1.62		2.35		1.36		.86	
2.00	.89		.65		.64		1.05		1.52		.94		.64	
5.00	.49		.48		.38		.68		.73		.53		.39	
10.00	.29	A	.25		.23		.34		.32		.30		.24	
20.00	.15	A	.13		.11		.16		.06		.14		.12	
30.00	.08		.03		.06		.08		.01		.07		.05	
40.00	-.01		.01		.02		.00		-.01		.00		.02	
50.00	0.00		0.00		0.00		0.00		0.00		0.00		0.00	
60.00	.03		.01		-.00		.01		.03		.01		.00	
70.00	.02		.36		.06		-.00		.04		.02		.06	
80.00	-.01		.06		.06	A	-.05		-.01		-.01		.06	
90.00	-.14		-.03		-.03	A	-.24		-.28		-.18		-.02	A
95.00	-.40		-.21		-.21	A	-.57		-.76		-.46		-.21	
98.00	-.94		-.56		-.57		-1.23		-1.72		-1.02		-.57	
99.00	-1.51		-.35		-.98		-1.98		-2.67		-1.58		-.91	
99.50	-2.19		-1.38		-1.31		-2.71		-3.95		-2.21		-1.33	
99.88	-3.44		-2.31		-1.86		-4.23		-6.03		-3.31		-1.98	
99.90	-4.67		-2.40		-2.27		-5.67		-7.56		-4.33		-2.32	
99.95	-6.29		-3.37		-2.67		-7.44		-9.91		-5.73		-2.80	

HAMILTON ATS-3　　　　　ALL DATA　　1969-72　　　LCCAL TIME
K=0-3

DIURNAL VARIATION

SI	00-24 PCT	10-14 PCT	14-18 PCT	18-22 PCT	22-02 PCT	02-06 PCT	06-10 PCT
00-19	86.61	94.57	94.24	85.66	72.65	79.49	92.92
20-39	8.00	4.40	5.26	8.90	11.76	11.70	5.95
43-59	2.77	.70	.43	2.76	7.05	4.77	.90
60-79	1.43	.15	.06	1.33	4.31	2.55	.19
80-89	.45	16	.01	.63	1.30	.69	.03
90-99	.74	..?	3.00	.72	2.93	.80	.01

DIURNAL VARIATION

PCT	08-24 DB X	10-14 DB X	14-18 DB X	18-22 DB X	22-02 DB X	02-06 DB X	06-10 DB X
.05	5.80	2.25	1.96	5.01	7.11	5.22	2.29
.10	4.05	1.78	1.62	4.07	6.00	4.31	1.88
.20	3.10	1.40	1.32	3.13	4.51	3.43	1.50
.50	2.92	.98	.96	2.05	3.61	2.38	1.08
1.00	1.39	.70	.73	1.42	2.61	1.72	.81
2.00	.91	.51	.53	.94	1.75	1.18	.58
5.00	.46	.29	.31	.49	.90	.65	.33
18.00	.24	.17	.18	.26	.45	.35	.19
29.00	.18	.08	.08	.11	.15	.15	.08
30.00	.05	.04	.04	.05	.05	.07	.03
40.00	-.01	.06	.01	-.01	.01	.01	.01
50.90	0.00	0.00	0.00	0.00	8.00	8.00	8.00
68.00	.03	.02	.01	.03	.01	.00	.01
70.00	.04	.09	.09	.03	-.01	.01	.00
80.00	.02	.12	.11 A	.01	-.10	-.05	.09 A
98.00	-.12	.39 A	.07 A	-.14	-.43	-.28	.03 A
95.00	-.40	-.05	-.07 A	-.43	-.57	-.64	-.14 A
98.00	-.98	-.36	-.39	-1.02	-2.00	-1.34	-.49
99.00	-1.60	-.67	-.66	-1.64	-2.99	-2.00	-.82
99.50	-2.33	-1.39	-1.06	-2.38	-4.31	-2.76	-1.25
99.80	-3.67	-1.69	-1.61	-3.74	-6.53	-4.10	-1.63
99.90	-4.95	-2.18	-2.02	-5.03	-8.45	-5.34	-2.30
99.95	-6.68	-2.68	-2.41	-6.71	-10.44	-7.04	-2.76

HAMILTON ATS-3　　　　　ALL DATA　　1969-72　　　LOCAL TIME
K=4,9

DIURNAL VARIATION

SI	00-24 PCT	10-14 PCT	14-18 PCT	18-22 FCT	22-02 PCT	02-06 PCT	06-10 PCT
00-19	75.28	93.31	89.26	79.05	60.54	53.15	78.12
20-39	13.56	5.72	7.72	10.79	19.13	21.59	17.23
40-59	5.09	1.33	2.25	4.29	7.16	12.59	2.07
60-79	2.65	.24	.63	2.46	4.75	6.06	1.29
80-89	1.13	0.30	.07	.95	2.91	2.15	.30
93-99	2.28	0.00	.67	2.46	5.51	4.48	.20

DIURNAL VARIATION

PCT	08-24 DB X	10-14 DB X	14-18 CB X	18-22 CB X	22-02 DB X	02-06 DB X	06-10 DB X
.05	6.72	2.27	3.88	6.62	7.81	7.62	3.81
.10	5.60	1.88	2.46	5.68	7.01	6.69	3.13
.20	4.54	1.52	1.96	4.61	5.90	5.57	2.51
.50	3.28	1.39	1.40	3.23	4.58	4.22	1.88
1.00	2.25	.81	1.04	2.22	3.43	3.28	1.37
2.00	1.48	.56	.73	1.42	2.39	2.28	1.02
5.00	.77	.30	.41	.68	1.85	1.39	.65
10.00	.40	.16	.27	.32	.65	.75	.42
20.00	.17	.06	.09	.18	.24	.36	.22
38.00	.08	.03	.04	.03	.10	.10	.09
48.00	.00	.01	.01	-.02	.02	.06	.03
50.00	0.00	0.90	0.00	0.00	8.00	0.00	8.00
60.00	.00	.01	.01	.02	-.01	-.05	-.02
70.05	-.02	.09	.06	.02	-.07	-.14	-.03
80.00	-.09	.11 A	.05	-.03	-.22	-.33	-.18
98.00	-.36	.04 A	-.07	-.27	-.68	-.00	-.31
95.00	-.81	-.12 A	-.29	-.78	-1.39	-1.46	-.61
98.00	-1.69	-.48	-.71	-1.68	-2.71	-2.60	-1.15
99.00	-2.58	-.92	-1.17	-2.53	-4.12	-3.79	-1.63
99.50	-3.80	-1.25	-1.65	-3.82	-5.76	-5.25	-2.17
99.80	-5.85	-1.83	-2.33	-5.97	-8.30	-7.72	-2.96
99.90	-7.78	-2.29	-2.92	-7.94	-18.31	-9.65	-3.77
99.95	-9.72	-2.74	-3.61	-9.92	-12.40 A	-12.01	-4.54

NARSSARSSUAQ ATS-3   NOV-JAN   1968-72   LCCAL TIHE
K=0-3

CIURNAL VARIATION

SI	00-24 PCT	10-14 PCT	14-18 PCT	18-22 PCT	22-02 PCT	02-06 PCT	06-10 PCT
00-19	35.83	41.74	29.15	33.29	23.65	35.78	51.94
20-39	29.37	31.39	28.56	32.07	38.59	25.38	27.52
40-59	16.32	13.51	18.51	19.41	18.50	15.63	12.85
60-79	9.22	6.89	11.70	8.93	12.01	10.03	5.68
80-89	3.94	2.66	5.08	3.80	5.81	5.54	1.61
90-99	5.32	3.31	7.08	3.30	9.36	7.63	1.30

DIURNAL VARIATION

PCT	00-24 DB	X	10-14 DB	X	14-18 DB	X	18-22 DB	X	22-02 DB	X	02-06 DB	X	06-10 DB	X
.05	7.82		7.37		8.03	B	7.41		7.96	B	8.08	B	6.13	
.10	7.06		6.32		7.41		6.38		7.68		7.48		5.05	
.20	5.94		5.22		6.39		5.26		6.82		6.50		4.20	
.50	4.54		3.96		4.94		4.84		5.32		5.04		3.13	
1.00	3.68		3.03		3.98		3.15		4.32		4.06		2.41	
2.00	2.65		2.21		2.99		2.36		3.29		3.04		1.79	
5.00	1.68		1.34		1.84		1.48		2.02		1.83		1.12	
10.00	.99		.84		1.14		.96		1.25		1.09		.70	
20.03	.49		.42		.57		.50		.63		.52		.35	
30.00	.25		.21		.29		.26		.32		.26		.18	
40.00	.10		.09		.12		.11		.13		.10		.07	
50.00	0.00		0.00		0.00		0.00		0.00		0.00		0.00	
60.00	-.18		-.08		-.12		-.11		-.13		-.10		-.07	
70.00	-.25		-.21		-.38		-.25		-.33		-.25		-.17	
80.00	-.51		-.43		-.60		-.52		-.67		-.53		-.34	
90.00	-1.08		-.91		-1.26		-1.05		-1.39		-1.20		-.75	
95.00	-1.63		-1.53		-2.09		-1.78		-2.38		-2.08		-1.26	
97.00	-3.08		-2.55		-3.52		-2.73		-3.92		-3.59		-2.09	
99.00	-4.34		-3.59		-4.88		-3.75		-5.44		-5.03		-2.82	
99.50	-5.85		-4.34		-5.58		-4.93		-7.29		-6.78		-3.74	
99.80	-8.31		-7.37		-9.06		-7.12		-9.84		-9.28		-5.15	
99.90	-10.26		-8.91		-11.14		-8.94		-12.19		-11.43		-6.78	
99.95	-12.39	A	-10.93		-13.94		-10.94		-15.14	A	-14.45		-8.46	

NARSSARSSUAQ ATS-3   FEB-APR   1968-72   LCCAL TIHE
K=8-3

CIURNAL VARIATION

SI	00-24 PCT	10-14 PCT	14-18 PCT	18-22 PCT	22-02 PCT	02-06 PCT	06-10 PCT
00-19	24.15	45.36	28.89	9.41	5.31	11.38	42.13
20-39	22.72	32.69	29.42	13.38	5.85	18.88	32.67
40-59	14.77	13.49	17.95	15.89	12.48	16.65	13.1
60-79	11.78	4.57	11.14	14.72	16.51	17.03	6.4
80-89	6.78	1.21	4.65	11.88	11.66	10.39	2.3
90-99	19.89	2.08	8.34	36.48	45.18	25.04	3.10

DIURNAL VARIATION

PCT	00-24 DB	X	10-14 CB	X	14-18 DB	X	18-22 DB	X	22-02 DB	X	02-06 DB	X	06-10 DB	X
.05	7.15	B	6.65		6.13	B	6.67	B	6.13	B	7.21	B	7.26	
.10	8.04	B	5.33		7.55		7.51	B	7.78	B	7.86	B	6.21	
.20	7.68		4.50		6.60		8.21	B	8.07	B	7.94		5.11	
.50	6.42		3.32		5.13		7.31		7.55		6.87		3.87	
1.00	5.31		2.52		4.15		6.26		6.50		5.75		2.95	
2.00	4.27		1.85		3.11		5.15		5.48		4.66		2.14	
5.00	2.75		1.16		1.89		3.72		4.06		3.22		1.31	
10.00	1.64		.75		1.16		2.49		2.83		2.07		.82	
20.00	.75		.38		.57		1.27		1.54		1.64		.41	
30.00	.36		.20		.29		.65		.81		.53		.21	
40.00	.14		.08		.12		.27		.34		.22		.08	
50.00	0.00		0.00		0.00		0.00		0.00		0.00		0.00	
60.00	-.14		-.08		-.12		-.27		-.34		-.22		-.08	
70.00	-.36		-.19		-.38		-.68		-.84		-.56		-.21	
80.00	-.08		-.39		-.68		-1.38		-1.66		-1.12		-.42	
90.00	-1.82		-.96		-1.28		-2.79		-3.21		-2.32		-.89	
95.00	-3.13		-1.32		-2.15		-4.51		-5.02		-3.80		-1.49	
98.00	-5.36		-2.18		-3.67		-7.03		-7.62		-6.09		-2.47	
99.00	-7.31		-3.95		-5.13		-8.98		-9.61		-8.07		-3.48	
99.50	-9.25		-3.98		-6.95		-11.16		-12.02		-10.07		-4.68	
99.80	-12.36		-5.74		-9.48		-15.15	A	-14.03	B	-13.72		-6.87	
99.90	-15.08		-7.60		-11.78		3.10	B	28.58	B	-12.67	B	-8.71	
99.95	9.20	B	-9.48		-15.64	A	98.68	C	139.51	B	35.60	B	-10.78	

NARSSARSSUAQ ATS-3   MAY-JUL   1968-72   LOCAL TIME
K=0-3

DIURNAL VARIATION

SI	00-24 PCT	10-14 PCT	14-18 PCT	18-22 PCT	22-02 PCT	02-06 PCT	06-10 PCT
00-19	34.56	64.47	51.32	13.78	3.76	13.75	59.50
20-39	21.22	27.43	28.16	17.92	6.60	22.43	24.78
40-59	12.87	6.38	12.23	16.97	10.91	22.85	8.19
60-79	10.65	.89	4.49	17.29	18.57	18.37	4.56
80-89	6.99	.34	1.71	10.80	18.23	9.63	1.35
90-99	13.72	.48	2.09	23.25	41.93	12.98	1.62

DIURNAL VARIATION

PCT	00-24 DB	X	10-14 DB	X	14-18 DB	X	18-22 DB	X	22-02 DB	X	02-06 DB	X	06-10 DB	X
.05	7.71	B	4.42		6.72		6.51	B	6.08	B	7.56	B	6.33	
.10	8.00		3.59		5.59		7.93	B	7.11	B	7.97		5.22	
.20	7.29		2.90		4.56		7.85		8.05	B	7.30		4.29	
.50	5.88		2.12		3.37		6.71		7.50		5.89		3.12	
1.00	4.79		1.64		2.55		5.60		6.52		4.81		2.33	
2.00	3.77		1.24		1.85		4.53		5.41		3.84		1.67	
5.00	2.30		.52		1.14		3.10		4.01		2.50		1.01	
10.00	1.34		.52		.70		1.98		2.82		1.60		.62	
20.00	.59		.27		.35		.99		1.59		.84		.32	
33.00	.25		.14		.17		.51		.86		.44		.14	
40.00	.10		.06		.07		.21		.37		.19		.05	
50.00	0.00		0.00		0.00		0.00		0.00		0.00		0.00	
60.00	-.10		-.35		-.08		-.21		-.38		-.19		-.05	
70.00	-.25		-.12		-.17		-.53		-.50		-.46		-.12	
80.00	-.60		-.23		-.34		-1.06		-1.73		-.90		-.27	
90.00	-1.47		-.51		-.75		-2.21		-3.23		-1.79		-.62	
95.00	-2.60		-.98		-1.28		-3.63		-4.98		-2.86		-1.11	
98.00	-4.58		-1.47		-2.17		-5.85		-7.49		-4.68		-1.95	
99.00	-6.33		-1.99		-2.98		-7.80		-9.45		-6.34		-2.70	
99.50	-8.28		-2.53		-4.06		-9.77		-11.78		-8.23		-3.71	
99.80	-10.98		-3.50		-5.87		-12.66		-14.74	B	-10.85		-5.33	
99.90	-13.73		-4.35		-7.70		-13.66	B	13.40	B	-13.25		-7.05	
99.95	-10.11	B	-5.61		-9.57		23.11	B	119.97	B	-11.63	B	-8.87	

NARSSARSSUAQ ATS-3   AUG-OCT   1968-72   LOCAL TIME
K=0-3

DIURNAL VARIATION

SI	00-24 PCT	10-14 PCT	14-18 PCT	18-22 PCT	22-02 PCT	02-06 PCT	06-10 PCT
00-19	34.36	53.58	46.63	16.38	7.19	23.16	59.52
20-39	23.03	27.12	26.80	16.83	15.24	27.28	24.79
40-59	16.31	10.39	12.55	19.63	22.55	21.66	10.40
60-79	11.75	4.57	8.43	18.87	22.68	11.92	3.92
80-89	6.04	1.91	3.27	11.22	12.89	5.87	1.05
90-99	8.51	1.73	2.30	17.08	19.43	18.11	.33

DIURNAL VARIATION

PCT	00-24 DB	X	10-14 DB	X	14-18 DB	X	18-22 DB	X	22-02 DB	X	02-06 DB	X	06-10 DB	X
.05	8.14	6	6.50		7.09		7.11	B	6.70	B	7.53	B	4.68	
.10	7.60		5.39		5.95		8.14	B	7.96	B	7.75		4.03	
.20	6.67		4.46		4.69		7.58		7.72		6.92		3.37	
.50	5.28		3.26		3.76		6.29		6.50		5.44		2.56	
1.00	4.22		2.48		2.91		5.18		5.39		4.42		2.01	
2.00	3.19		1.80		2.15		4.19		4.38		3.38		1.52	
5.00	1.94		1.16		1.32		2.78		2.99		2.09		.96	
10.00	1.17		.68		.81		1.78		1.97		1.30		.61	
20.00	.56		.33		.48		.90		1.06		.66		.31	
33.00	.27		.17		.20		.47		.57		.34		.16	
40.00	.11		.37		.08		.19		.24		.14		.07	
50.00	0.00		0.00		0.00		0.00		0.00		0.00		0.00	
60.00	-.10		-.36		-.07		-.19		-.25		-.14		-.06	
70.00	-.26		-.15		-.19		-.48		-.60		-.35		-.14	
80.00	-.58		-.32		-.39		-.96		-1.14		-.76		-.27	
90.00	-1.29		-.72		-.87		-1.99		-2.21		-1.44		-.63	
95.00	-2.21		-1.24		-1.49		-3.21		-3.58		-2.38		-1.06	
98.00	-3.79		-2.11		-2.48		-5.23		-5.55		-4.04		-1.78	
99.00	-5.27		-2.89		-3.44		-7.85		-7.41		-5.60		-2.37	
99.50	-7.07		-3.92		-4.53		-8.94		-9.31		-7.48		-3.04	
99.80	-9.58		-5.60		-6.46		-11.88		-12.32		-10.86		-4.07	
99.90	-11.08		-7.32		-8.28		-15.01	A	-15.80		-12.23		-4.85	
99.95	-14.99	A	-9.14		-10.02		-1.89	B	7.28	B	-15.88	B	-6.84	

NARSSARSSUAQ ATS-3   ALL DATA   1968-72   LOCAL TIME
K=0-3

DIURNAL VARIATION

SI	00-24 PCT	10-14 PCT	14-18 PCT	18-22 PCT	22-02 PCT	02-06 PCT	06-10 PCT
00-19	32.07	50.39	37.34	19.57	10.98	21.50	52.14
20-39	24.53	30.31	28.32	21.32	16.07	23.05	27.90
40-59	15.00	11.33	15.88	17.67	15.46	18.61	11.11
60-79	10.63	4.39	9.21	14.01	16.53	14.39	5.43
80-89	5.81	1.56	3.81	8.28	11.72	7.97	1.66
90-99	11.96	2.32	5.43	19.15	29.25	14.48	1.76

DIURNAL VARIATION

PCT	00-24 DB	X	10-14 DB	X	14-18 DB	X	18-22 DB	X	22-02 DB	X	02-06 DB	X	06-10 DB	X
.05	7.85	B	6.65		7.83		7.09	B	7.00	B	7.54	B	6.51	
.10	7.68		5.53		7.08		8.02	B	7.74	B	8.04	B	5.40	
.20	7.11		4.51		5.96		7.66		8.04	B	7.38		4.42	
.50	5.66		3.32		4.56		6.39		7.04		5.99		3.28	
1.00	4.59		2.51		3.62		5.28		5.94		4.90		2.50	
2.00	3.56		1.82		2.66		4.25		4.85		3.89		1.83	
5.00	2.14		1.12		1.60		2.77		3.41		2.48		1.12	
10.00	1.26		.70		.98		1.71		2.23		1.53		.70	
20.00	.58		.35		.48		.82		1.13		.75		.34	
30.00	.28		.18		.24		.41		.58		.38		.17	
40.00	.11		.07		.10		.17		.24		.15		.07	
50.00	0.00		0.00		0.00		0.00		0.00		0.00		0.00	
60.00	-.10		-.07		-.09		-.16		-.24		-.15		-.06	
70.00	-.27		-.17		-.24		-.42		-.60		-.39		-.16	
80.00	-.61		-.35		-.50		-.88		-1.21		-.79		-.33	
90.00	-1.39		-.75		-1.07		-1.90		-2.49		-1.69		-.74	
95.00	-2.42		-1.27		-1.82		-3.18		-4.07		-2.82		-1.26	
98.00	-4.27		-2.13		-3.08		-5.34		-6.43		-4.76		-2.13	
99.00	-5.95		-2.93		-4.35		-7.25		-8.41		-6.53		-2.92	
99.50	-7.90		-3.98		-5.88		-9.17		-10.42		-8.45		-3.93	
99.80	-10.52		-5.77		-8.35		-12.24		-14.14		-11.19		-5.59	
99.90	-12.77		-7.60		-10.31		-15.12	A	-7.99	B	-14.88		-7.32	
99.95	-13.23	B	-9.46		-12.44	A	6.30	B	52.01	B	-8.39	B	-9.13	

NARSSARSSUAQ ATS-3   ALL DATA   1968-72   LOCAL TIME
K=4-9

DIURNAL VARIATION

SI	00-24 PCT	10-14 PCT	14-18 PCT	18-22 PCT	22-02 PCT	02-06 PCT	06-10 PCT
00-19	8.45	20.66	12.61	5.38	1.14	1.46	13.37
20-39	11.75	21.76	17.59	9.64	3.86	4.90	16.23
40-59	14.36	18.41	17.54	14.88	9.19	9.63	18.31
60-79	16.00	13.47	15.89	18.36	15.92	16.11	15.46
80-89	12.26	9.30	11.26	12.56	14.04	14.48	10.52
90-99	37.18	15.38	25.21	39.17	55.86	53.41	26.11

DIURNAL VARIATION

PCT	00-24 DB	X	10-14 DB	X	14-18 DB	X	18-22 DB	X	22-02 DB	X	02-06 DB	X	06-10 DB	X
.05	6.56	B	7.39	B	6.32	B	6.38	B	5.52	B	5.63	B	7.23	B
.10	7.45	B	8.11	B	7.88	B	7.33	B	7.41	B	7.47	B	7.87	B
.20	8.13	B	7.45		7.92		8.05	B	7.57	B	7.59	B	7.95	
.50	7.34		6.15		6.85		7.48		7.78		7.74		6.89	
1.00	6.30		5.35		5.72		6.38		6.92		6.87		5.76	
2.00	5.19		4.04		4.64		5.27		5.81		5.75		4.68	
5.00	3.77		2.61		3.20		3.86		4.39		4.33		3.23	
10.00	2.55		1.51		2.06		2.65		3.19		3.12		2.08	
20.00	1.32		.79		1.03		1.43		1.86		1.81		1.03	
30.00	.68		.40		.53		.75		1.03		.99		.53	
40.00	.28		.18		.22		.32		.45		.43		.22	
50.00	0.00		0.00		0.00		0.00		0.00		0.00		0.00	
60.00	-.29		-.16		-.22		-.32		-.46		-.44		-.22	
70.00	-.71		-.41		-.55		-.79		-1.09		-1.04		-.55	
80.00	-1.44		-.94		-1.11		-1.54		-2.02		-1.96		-1.11	
90.00	-2.87		-1.80		-2.30		-2.99		-3.72		-3.63		-2.32	
95.00	-4.58		-2.39		-3.77		-4.71		-5.56		-5.45		-3.81	
98.00	-7.10		-5.31		-6.65		-7.25		-8.21		-8.10		-6.11	
99.00	-9.05		-6.32		-8.02		-9.20		-10.27		-10.13		-8.18	
99.50	-11.24		-8.72		-10.01		-11.44		-12.52		-12.39	A	-10.18	
99.80	-15.15	A	-11.61		-13.05		-15.00		-9.51	B	-10.82	B	-13.29	
99.90	4.32	B	-15.12		-12.23	B	8.07	B	45.81	B	39.78	B	-11.42	B
99.95	94.34	B	-4.73	B	32.11	B	105.41	B	200.19	B	186.07	B	36.51	B

THULE .S-3   ALL DATA   1968-70   LCCAL TIME
K=0-3

DIURNAL VARIATION

SI	00-24 PCT	10-14 PCT	14-18 PCT	18-22 PCT	22-02 PCT	02-06 PCT	06-10 PCT
00-19	1.28	4.10	1.35	0.00	0.00	.17	2.03
20-39	4.64	7.55	5.40	2.42	.08	3.90	8.52
40-59	14.61	15.09	19.49	11.77	7.04	15.68	18.23
60-79	28.92	25.92	27.59	28.79	27.27	35.17	28.95
80-89	23.46	19.77	23.12	24.84	24.58	21.95	22.11
90-99	27.10	27.07	23.04	32.18	36.68	23.14	20.17

DIURNAL VARIATION

PCT	00-24 DB	X	10-14 DB	X	14-18 DB	X	18-22 DB	X	22-02 DB	X	02-06 DB	X	06-10 DB	X
.05	5.38	B	5.56	B	5.91	B	6.24	B	5.92	B	5.72	B	6.26	B
.10	7.57	B	7.64	B	7.75	B	7.33	B	7.08	B	7.70	B	7.85	B
.20	8.0A	B	8.30		7.90		8.12	B	8.00	B	7.90		7.80	
.50	7.07		7.34		6.88		7.27		7.42		6.89		6.69	
1.00	5.97		5.33		5.76		6.21		6.42		5.76		5.58	
2.00	4.89		4.85		4.59		5.12		5.32		4.70		4.54	
5.00	3.56		3.48		3.37		3.77		3.56		3.39		3.23	
10.00	2.48		2.40		2.34		2.66		2.04		2.37		2.23	
20.00	1.43		1.34		1.35		1.56		1.70		1.39		1.27	
30.00	.81		.74		.76		.90		1.00		.79		.71	
40.00	.36		.32		.33		.40		.45		.35		.31	
50.00	0.00		0.30		0.00		0.00		0.00		0.00		0.00	
60.00	-.37		-.33		-.35		-.41		-.46		-.37		-.32	
70.00	-.85		-.77		-.80		-.95		-1.05		-.84		-.75	
80.00	-1.55		-1.45		-1.46		-1.70		-1.86		-1.50		-1.38	
90.00	-2.82		-2.71		-2.65		-3.05		-3.29		-2.68		-2.52	
95.00	-4.30		-4.20		-4.06		-4.61		-4.92		-4.07		-3.87	
98.00	-6.52		-6.43		-6.16		-6.93		-7.29		-6.16		-5.89	
99.00	-8.39		-8.33		-8.01		-8.82		-J.19		-8.00		-7.69	
99.50	-10.34		-10.31		-9.91		-10.83		-11.29		-9.90		-9.56	
99.80	-13.64		-13.64		-12.63		-16.12	A	-15.14	A	-12.56		-12.28	
99.90	-10.55	B	-10.35	B	-13.82	B	-4.19	B	3.03	B	-13.76	B	-15.00	B
99.95	40.00	B	40.24	B	21.21	B	65.61	B	89.28	B	21.73	B	9.41	B

THULE ATS-3   ALL DATA   1968-70   LOCAL TIME
K=4,9

CIURNAL VARIATION

SI	00-24 PCT	10-14 PCT	14-18 PCT	18-22 PCT	22-02 PCT	02-06 PCT	06-10 PCT
00-19	0.00	0.30	0.00	0.00	0.00	0.00	0.00
20-39	1.55	2.34	1.33	0.00	0.00	4.62	0.00
40-59	7.43	1.47	9.33	7.59	12.59	6.15	4.35
60-79	30.40	26.47	45.33	30.38	32.59	23.85	27.17
80-89	31.61	33.82	22.67	32.91	29.63	38.46	29.35
90-99	29.02	35.29	21.33	29.11	25.19	26.92	39.13

CIURNAL VARIATION

PCT	00-24 DB	X	10-14 DB	X	14-18 DB	X	18-22 DB	X	22-02 DB	X	02-06 DB	X	06-10 DB	X
.05	4.94	B	5.93	B	5.65	B	4.90	B	5.38	B	5.24	B	5.77	B
.10	7.39	B	7.16	B	7.70	B	7.38	B	7.57	B	7.49	B	6.96	B
.20	8.06	B	8.30	B	7.86		8.06	B	7.97		8.02	B	8.00	B
.50	7.20		7.46		6.83		7.21		7.05		7.16		7.48	
1.00	6.14		6.40		5.69		6.15		5.55		6.10		6.51	
2.00	5.05		5.30		4.64		5.06		4.87		5.01		5.48	
5.00	3.73		3.96		3.37		3.75		3.58		3.71		4.04	
10.00	2.66		2.95		2.39		2.68		2.54		2.66		2.92	
20.00	1.59		1.72		1.43		1.61		1.52		1.59		1.75	
30.00	.93		1.30		.83		.95		.88		.92		1.03	
40.00	.42		.45		.37		.43		.40		.41		.47	
50.00	0.00		0.10		0.00		0.00		0.00		0.00		0.00	
60.00	-.43		-.46		-.38		-.44		-.41		-.42		-.48	
70.00	-.96		-1.06		-.87		-1.00		-.93		-.97		-1.09	
80.00	-1.74		-1.95		-1.53		-1.77		-1.65		-1.74		-1.93	
90.00	-3.07		-3.32		-2.69		-3.18		-2.90		-3.08		-3.39	
95.00	-4.58		-4.33		-4.34		-4.61		-4.35		-4.59		-5.04	
98.00	-6.80		-7.25		-6.04		-6.82		-6.48		-6.74		-7.45	
99.00	-8.65		-9.14		-7.85		-8.60		-8.21		-8.57		-9.36	
99.50	-10.57		-11.19		-9.78		-10.59		-19.21		-10.43		-11.58	
99.80	-14.89		-15.39	A	-12.39	A	-14.11		-13.85		-13.60		-15.00	
99.90	-8.50	B	.54	B	-14.63	B	-8.39	B	-12.35	B	-10.84	B	7.52	B
99.95	43.59	B	80.39	B	14.02	B	48.94	B	30.33	B	37.86	B	102.58	B